GEORGIA INSTITUTE OF TECHNOLOGY
OFFICE OF CONTRACT ADMINISTRATION
SPONSORED PROJECT INITIATION

Date: November 17, 1980

Project Title: Coherent Polarization-Diversity Radar Measurements of Clouds and Precipitation

Project No: A-2818

Project Director: Dr. James I. Metcalf

Sponsor: National Science Foundation

Agreement Period: From 11/1/80 Until 10/31/82 (Grant Period)

Type Agreement: Grant No. ATM-8018382, dated October 29, 1980

Amount: $71,600 NSF (A-2818)
724 GIT (E-702-808)
$72,324 TOTAL

Reports Required: Annual Progress Report (w/renewal proposal); Final Project Report

Sponsor Contact Person (s):

Technical Matters

NSF Program Official
L. Randall Koenig
Associate Program Director
Meterology Program
Atmospheric Research Section
Division of Atmospheric Sciences
Directorate for Astronomical, Atmospheric, Earth, and Ocean Sciences
National Science Foundation
Washington, D. C. 20550
202/357-7624

Contractual Matters
(thru OCA)

NSF Grants Official
Lee A. De Herrera
Section II, AAEO/EAS Branch
Division of Grants and Contracts
Directorate for Administration
National Science Foundation
Washington, D. C. 20550
202/357-9602

Defense Priority Rating: N/A

Assigned to: RAIL/RAD (School/Laboratory)

COPIES TO:

Project Director
Division Chief (EES)
School/Laboratory Director
Dean/Director–EES
Accounting Office
Procurement Office
Security Coordinator (OCA)
Reports Coordinator (OCA)

Library, Technical Reports Section
EES Information Office
EES Reports & Procedures
Project File (OCA) 11/19/80 ed
Project Code (GTRI)
Other

GEORGIA INSTITUTE OF TECHNOLOGY OFFICE OF CONTRACT ADMINISTRATION

SPONSORED PROJECT TERMINATION SHEET

Date 11/12/82

Project Title: Coherent Polarization-Diversity Radar Measurements of Clouds and Precipitation

Project No: A-2818

Project Director: J. D. Echard

Sponsor: NSF

Effective Termination Date: 10/31/82

Clearance of Accounting Charges: 10/31/82

Grant/Contract Closeout Actions Remaining:

- [ ] Final Invoice and Closing Documents
- [x] Final Fiscal ~~Report~~ Accounting (FCTR)
- [ ] Final Report of Inventions
- [ ] Govt. Property Inventory & Related Certificate
- [ ] Classified Material Certificate
- [ ] Other _____

Assigned to: RAIL/AD (~~School~~/Laboratory)

COPIES TO:

Administrative Coordinator	Research Security Services	EES Public Relations (2)
Research Property Management	Reports Coordinator (OCA)	Computer Input
Accounting	Legal Services (OCA)	Project File
Procurement/EES Supply Services	Library	Other _____

APPENDIX VI

NATIONAL SCIENCE FOUNDATION
Washington, D.C. 20550

FINAL PROJECT REPORT
NSF FORM 98A

PLEASE READ INSTRUCTIONS ON REVERSE BEFORE COMPLETING

PART I–PROJECT IDENTIFICATION INFORMATION

1. Institution and Address	2. NSF Program	3. NSF Award Number
Radar Application Div. RAIL, EES Ga. Institute of Technology Atlanta, GA 30332		ATM-8018382
	4. Award Period From 11-2-80 To 10-31-82	5. Cumulative Award Amount $72,324

6. Project Title
Coherent Polarization - Diversity Radar Measurement of Clouds and Precipitation.

PART II–SUMMARY OF COMPLETED PROJECT *(FOR PUBLIC USE)*

The research performed was a continuation of the research reported by Metcalf and Echard (1978) and Metcalf (1980, 1981). The earlier work documented various theoretical and practical aspects of the interpretation of signals receivable by coherent polarization-diversity radars, including the formulation of the received signals and the spectral functions derivable from them and the effects of propagation phenomena, non-Rayleigh scattering, variations in apparent or actual shape and orientation of hydrometeors, and air velocity variance on the received signals and spectral functions.

To elucidate these effects we developed numerical simulations of the spectral functions incorporating air velocity variance, Mie scattering functions, and propagation effects. The simulation work also permitted us to develop and refine procedures for manipulating and displaying the spectral functions which could be used with spectral functions derived from radar data. Because of our expectation of having field data from the NOAA radar, we investigated characteristics of backscattered signals which might be encountered at 8.6-mm wavelength, namely, Mie scattering and non-negligible propagation effects. Scientific report No. 1 entitled "Numeric Simulation of Coherent Polarization - Diversity Radar Spectral Functions", documents the formulation of the model and presents initial results of the computations. This report, submitted in the form of an Interim Technical Report, 30 October 1981, also represents the final technical report on this project.

PART III–TECHNICAL INFORMATION *(FOR PROGRAM MANAGEMENT USES)*

1. ITEM *(Check appropriate blocks)*	NONE	ATTACHED	PREVIOUSLY FURNISHED	TO BE FURNISHED SEPARATELY TO PROGRAM	
				Check (√)	Approx. Date
a. Abstracts of Theses					
b. Publication Citations			X		
c. Data on Scientific Collaborators			X		
d. Information on Inventions	X				
e. Technical Description of Project and Results			X		
f. Other *(specify)*					

2. Principal Investigator/Project Director Name *(Typed)*	3. Principal Investigator/Project Director Signature	4. Date
Dr. J. D. Echard		9-21-82

NSF Form 98A (5-78) Supersedes All Previous Editions

Form Approved OMB No. 3145-0058

A-2818

SCIENTIFIC REPORT NO. 1
PROJECT A–2818

NUMERICAL SIMULATION OF COHERENT POLARIZATION–DIVERSITY RADAR SPECTRAL FUNCTIONS

By

James I. Metcalf
James E. Matthews III

Radar Applications Division
Radar and Instrumentation Laboratory

Prepared for

METEOROLOGY PROGRAM
DIVISION OF ATMOSPHERIC SCIENCES
NATIONAL SCIENCE FOUNDATION
WASHINGTON DC 20550

Grant No. ATM–8018382

30 October 1981

GEORGIA INSTITUTE OF TECHNOLOGY
A Unit of the University System of Georgia
Engineering Experiment Station
Atlanta, Georgia 30332

GTEES

1981

NUMERICAL SIMULATION OF COHERENT POLARIZATION-DIVERSITY RADAR SPECTRAL FUNCTIONS

BY

James I. Metcalf[1]
and
James E. Matthews III[2]

Prepared for

Meteorology Program
Division of Atmospheric Sciences
National Science Foundation
Washington DC 20550

Grant No. ATM-8018382

30 October 1981

Prepared by

Radar Applications Division
Engineering Experiment Station
Georgia Institute of Technology
Atlanta GA 30332

[1]Present affiliation: Air Force Geophysics Laboratory, Ground-Based Remote Sensing Branch, Hanscom AFB MA 01731

[2]Present affiliation: Corning Glass Works, Inc., Telecommunications Products Div., Corning NY 14831

TABLE OF CONTENTS

LIST OF FIGURES

I. INTRODUCTION

The research described in the following sections is a continuation of the research reported by Metcalf and Echard (1978) and Metcalf (1980, 1981). The earlier work documented various theoretical and practical aspects of the interpretation of signals receivable by coherent polarization-diversity radars, including the formulation of the received signals and the spectral functions derivable from them and the effects of propagation phenomena, non-Rayleigh scattering, variations in apparent or actual shape and orientation of hydrometeors, and air velocity variance on the received signals and spectral functions.

To elucidate these effects we developed numerical simulations of the spectral functions incorporating air velocity variance, Mie scattering functions, and propagation effects. The simulation work also permitted us to develop and refine procedures for manipulating and displaying the spectral functions which could be used with spectral functions derived from radar data. The numerical simulation work was originally conceived as a counterpart to empirical studies based on data from the 8.6-mm coherent polarization-diversity radar operated by the Wave Propagation Laboratory of the National Oceanic and Atmospheric Administration (NOAA). This radar was first operated during the spring and summer of 1981 in Montana as part of the Cooperative Convective Precipitation Experiment (CCOPE). As the field program progressed, it became evident that little or no suitable data would be available for the proposed empirical studies, due to the infrequent occurrence of suitable weather and to operational problems with the radar. Consequently, we proceeded with a more comprehensive development of the spectral function model.

The model computation follows generally the approach of Warner and Rogers (1977), who computed power spectra corresponding to those observed in the transmission and orthogonal channels of a 10-cm radar transmitting circular polarization. Because of our expectation of having field data from the NOAA radar, we investigated characteristics of backscattered signals which might be encountered at 8.6-mm wavelength, namely, Mie scattering and non-negligible propagation effects. This report documents the formulation of the model and presents initial results of the computations.

The results shown in Section III illustrate the effects of air velocity variance, noise, and differential propagation parameters on the spectral functions at a particular

elevation angle and two rainfall rates. These results illustrate the requirement for low noise in the received signals, so that the spectral power ratio S_1/S_2 and the modified cross-spectrum S_{12}/S_2 can provide useful information on backscatter characteristics across the Doppler velocity domain. Because the cross-spectrum is not affected by the presence of noise (in the model), the modified cross-spectrum is useful within a wider Doppler velocity domain than is the spectral power ratio. With increasing air velocity variance, the numerical characteristics of the spectral functions at all velocities tend to approach the characteristics of the corresponding integrated quantities. Since the first maximum and minimum of the Mie scatter cross-section occur at relatively large drop sizes at 8.6 mm radar wavelength, the spectral features associated with these extrema occur at Doppler velocities well above those of the spectral peaks; with increasing air velocity variance, these features appear at relatively higher Doppler velocities. Therefore, in the interpretation of spectra computed from experimental data, it will be necessary to make an adjustment for air velocity variance before particular features of the spectral functions can be identified with particular Doppler fall speed components. The separation of scattering and propagation parameters in the spectral functions, as postulated by Metcalf (1981), will also require an adjustment for air velocity variance. Further simulation studies will be necessary to evaluate this possibility.

II. NUMERICAL CONCEPTS

A. Spectral Function Formulations

The power spectra derived from signals in the transmission channel (S_1) and the orthogonal channel (S_2) and the cross-spectrum (S_{12}) of the two received signals can be expressed as

$$S_1(v)=\int_o^\infty \sigma(r,\phi)\ G(V(r)\sin\phi,\Sigma)\ N(r)$$

$$\times\left|\nu(r,\phi)e^{j(\delta(r,\phi)\pm 2\alpha(r,\phi))}+2pe^{j(\chi\pm 2\tau)}\right|^2 dr \qquad (1)$$

$$S_2(v)=\int_o^\infty \sigma(r,\phi)\ G(V(r)\sin\phi,\Sigma)\ N(r)\ dr \qquad (2)$$

$$S_{12}(v)=\int_o^\infty \sigma(r,\phi)\ G(V(r)\sin\phi,\Sigma)\ N(r)$$

$$\times\left[\nu(r,\phi)e^{j(\delta(r,\phi)\pm 2\alpha(r,\phi))}+2pe^{j(\chi\pm 2\tau)}\right]\ dr \qquad (3)$$

where v is the Doppler velocity defined as positive toward the radar, σ is the backscatter cross-section, r is the equivalent spherical radius of a drop, ϕ is the elevation angle, $N(r)$ is the drop size distribution function, ν is the ratio of backscattered amplitudes into the transmission and orthogonal channels from each scatterer, δ is the differential phase shift between the major and minor axes of each scatterer due to non-Rayleigh scattering, and α is the orientation angle or canting angle of each scatterer. The propagation term $2pe^{j(\chi\pm 2\tau)}$ is based on a model of an anisotropic (precipitation-filled) medium with symmetry axes rotated through an angle τ from the vertical and horizontal. The other propagation parameters are related to the total one-way differential attenuation ΔA and differential phase shift $\Delta\Phi$ in the medium to first-order approximation by

$$pe^{jX} = \tanh(0.0575\ \Delta A \pm j(\pi/360)\Delta\Phi). \tag{4}$$

The upper and lower signs in Equations (1) and (3) and elsewhere correspond to the transmission of right and left circular polarization, respectively. The velocity weighting function is defined by

$$G(V(r)\sin\phi,\Sigma) = \frac{1}{\Sigma\sqrt{2\pi}} \exp\left[-\frac{(v-V(r)\sin\phi-V_a)^2}{2\Sigma^2}\right] \tag{5}$$

where V(r) is the raindrop fall speed in calm air, V_a is the Doppler velocity component due to air velocity, and Σ^2 is the Doppler velocity variance due to turbulence or wind shear. We have assumed $V_a=0$ for convenience in our computations.

The spectra defined in Equations (1), (2), and (3) yield the relation

$$\eta = \int_{-\infty}^{\infty} S_2(v)\ dv \tag{6}$$

where η is the reflectivity in units of inverse length, i.e., cross-section per unit volume. For Rayleigh scattering the cross-section is given by

$$\sigma = 64\ \pi^5\ r^6\ |K|^2\ \lambda^{-4} \tag{7}$$

where K is the refractive index factor and λ is the radar wavelength, and the spectrum S_2 can be normalized to yield the reflectivity factor Z. For Mie scattering the cross-section is given by

$$\sigma = \pi\ |S_{11}(r,\phi) + S_{22}(r,\phi)|^2 \tag{8}$$

where S_{11} and S_{22} are the backscatter amplitude coefficients for signals of polarizations perpendicular and parallel, respectively, to the raindrop symmetry axis (which is assumed to be vertically oriented). For our computations, we used values of S_{11} and S_{22} computed by Oguchi and Hosoya (1974). These computations were based on the linear size-shape relation of Spilhaus (1948), rather than the more realistic Pruppacher and Pitter (1971) size-shape relation, and our results therefore cannot be strictly representative of what one might observe in nature.

Warner and Rogers (1977) computed power spectra up to proportionality for Rayleigh scattering from raindrops having shapes as described by Pruppacher and Pitter. Their computations included air velocity standard deviation, radar elevation angle, rainfall rate, and fraction of preferentially oriented scatterers as computational parameters. The elevation angle affects the relative significance of fall speed variance and air velocity variance, and the rainfall rate affects the drop size distribution through the assumed Marshall and Palmer (1948) distribution function. We included all these parameters in our model and added propagation distance as a parameter to simulate non-negligible differential propagation effects.

The functions of greatest interest are the power spectrum S_2 (in the channel opposite to the transmission channel), the spectral power ratio S_1/S_2, the normalized cross-spectrum $S_{12}/(S_1S_2)^{\frac{1}{2}}$, and the function S_{12}/S_2 which we have called the modified cross-spectrum. The latter function is of particular interest where propagation effects are present. Using results from Metcalf (1981), we can express two of these functions as

$$S_1/S_2 = \overline{v^2} + 4p^2 + 4\,\mathrm{Re}\left[pe^{-j(\chi\pm 2\tau)}\overline{ve^{j(\delta\pm 2\alpha)}}\right] \tag{9}$$

$$S_{12}/S_2 = \overline{ve^{j(\delta\pm 2\alpha)}} + 2pe^{j(\chi\pm 2\tau)}. \tag{10}$$

The normalized cross-spectrum is inherently more complicated, as it is related to the two functions above by

$$S_{12}/(S_1 S_2)^{\frac{1}{2}} = \frac{S_{12}/S_2}{(S_1/S_2)^{\frac{1}{2}}} \tag{11}$$

The overbars indicate integration over drop size, as shown explicity in Equations (1), (2), and (3). For modeling of the spectral functions, it is useful to express the averaged quantities in terms of parameters that allow some separation of variables, characterize the extent to which the medium is preferentially oriented, and characterize the orientation angle. Ultimately, it will be necessary to include the effect of shape variation on the backscatter power and amplitude ratios. The following subsections discuss in more detail the formulation of these ratios in the model.

B. Backscatter Amplitude Ratio

The backscatter amplitude ratio for an individual raindrop is defined analytically by

$$\nu_i e^{j\delta_i} = \frac{S_{11}-S_{22}}{S_{11}+S_{22}} \tag{12}$$

where S_{11} and S_{22} are the backscatter amplitude coefficients. The amplitude ratio shown in Figure 1 for two wavelengths and two elevation angles is based on the Oguchi and Hosoya amplitude coefficients. Comparing the curves for the two elevation angles at each wavelength, one can verify that the magnitude of the ratio is approximately proportional to $\cos^2\phi$ and that the phase angle δ is not strongly dependent on the elevation angle, except for drop diameters near half the wavelength, i.e., between about 4.0 and 4.5 mm diameter for 8.6-mm wavelength.

To evaluate the term $\overline{\nu e^{j(\delta \pm 2\alpha)}}$ for a collection of raindrops we use the approach of McCormick and Hendry (1975). We assume that drops of a given radius have a distribution of canting angles and integrate the quantity $\nu_i(r\phi)e^{j(\delta_i(r,\phi)\pm 2\alpha_i(r,\phi))}$ over all orientations to obtain the result

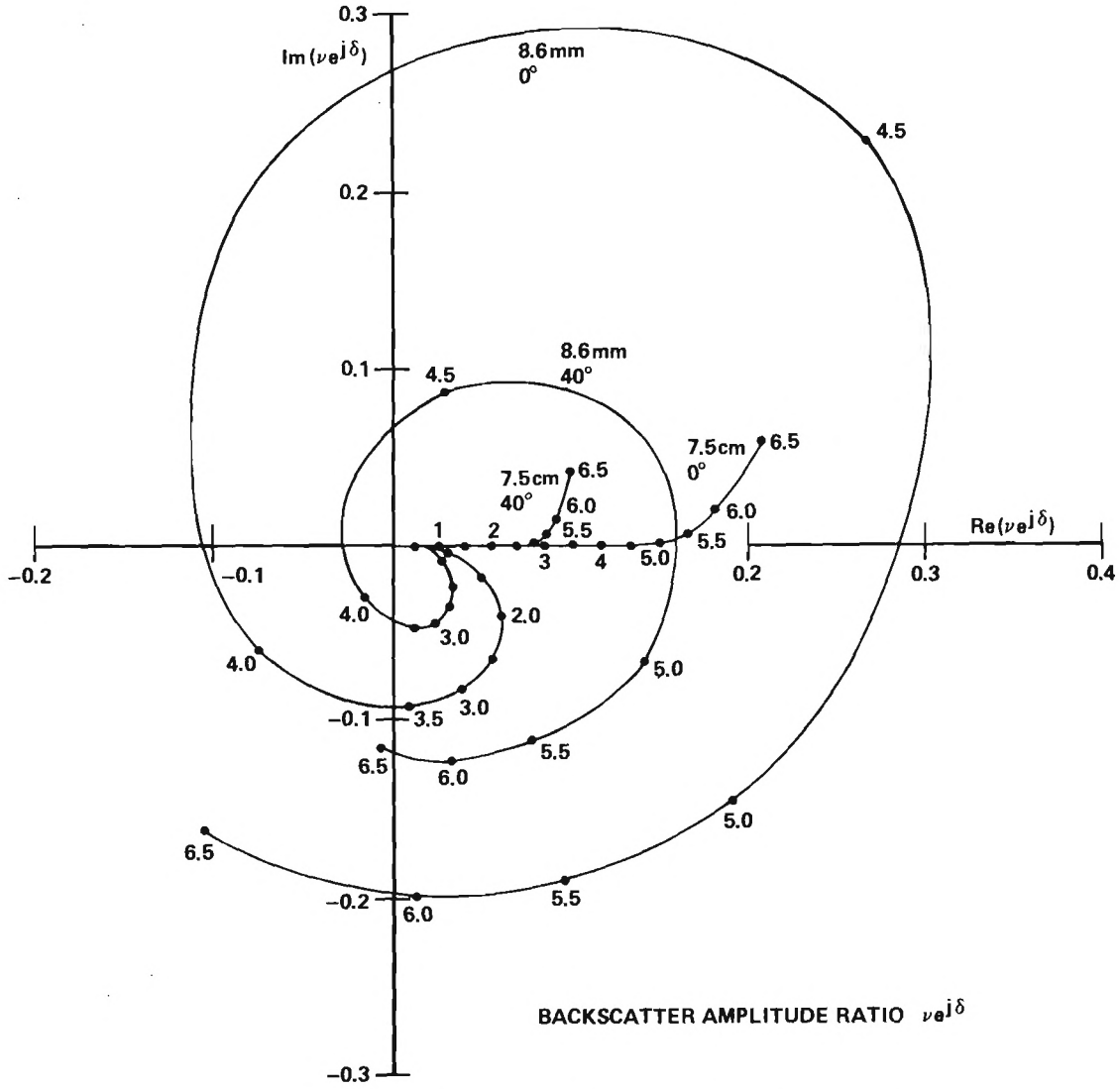

Figure 1. Backscatter amplitude ratio $\nu e^{j\delta}$ for raindrops, incorporating the Spilhaus size-shape relation and based on the scattering coefficients calculated by Oguchi and Hosoya. Calculations are shown for 0.5 mm increments of equivalent spherical diameter for wavelengths of 7.5 cm and 8.6 mm and elevation angles of 0^{o} and 40^{o}. Rayleigh scattering approximation holds for $D < 5$ mm at 7.5 cm wavelength and for $D < 0.6$ mm at 8.6 mm. Magnitude of ratio is approximately proportional to $\cos^{2}\phi$. Dependence of the phase shift δ on elevation angle is negligible for Rayleigh scattering but significant for drops with D/λ near 0.5.

$$\nu e^{j(\delta \pm 2\alpha)} = \rho_\alpha(r,\phi)\, \nu_i(r,\phi)\, e^{j(\delta_i(r,\phi) \pm 2\bar{\alpha}(r,\phi))} \tag{13}$$

where

$$\rho_\alpha(r,\phi) = \int_{-\pi/2}^{\pi/2} \cos\left[2(\alpha-\bar{\alpha})\right]\ T(\alpha-\bar{\alpha})\ d(\alpha-\bar{\alpha}) \tag{14}$$

$\bar{\alpha}$ is the average orientation angle, and $T(\alpha-\bar{\alpha})$ is the symmetrical distribution of canting angles. This result is equivalent to that corresponding to a medium having a fraction ρ_α of scatterers with a fixed orientation angle $\bar{\alpha}$ and a fraction $1-\rho_\alpha$ with a uniform random distribution of orientation angles. If either ρ_α or $\bar{\alpha}$ are independent of drop size, then they can be factored out of the implied integral in Equation (13). The quantities $\bar{\nu}$ and $\bar{\delta}$ can then be defined by

$$\bar{\nu} e^{j\bar{\delta}} = \frac{\int_0^\infty \sigma(r,\phi)\ N(r)\ G\ \nu(r,\phi) e^{j(\delta(r,\phi))}\ dr}{\int_0^\infty \sigma(r,\phi)\ N(r)\ G\ dr} \tag{15}$$

The use of $\bar{\nu}$ and $\bar{\delta}$ as separate parameters is of uncertain value, as the two cannot easily be modeled separately, except in the case of Rayleigh scattering where $\bar{\delta} \approx 0$. One can, however, approximately separate the size and elevation angle dependences of the quantities in Equation (13), since δ is approximately independent of elevation angle and $\nu_i(r,\phi) \approx \nu_i(r,0)\ \cos^2\phi$, where $\nu_i(r,0)$ is the amplitude ratio for a drop viewed perpendicular to its axis of rotational symmetry, i.e., horizontally.

In summary, the backscatter amplitude ratio for a collection of scatterers results only from those scatterers having a common orientation. The amplitude ratio for those scatterers can be computed either from the scattering amplitude coefficients for the specified radar elevation angle or (approximately) from the scattering amplitude coefficients for zero elevation angle. We use the former procedure in our computations.

C. Backscatter Power Ratio

We follow the approach of Warner and Rogers in formulating the backscatter power ratio. This quantity is the sum of two terms, corresponding to the preferentially oriented fraction ρ_α and the randomly oriented fraction $(1-\rho_\alpha)$, respectively. the power ratio can be expressed as

$$\nu^2(r,\phi) = \left[\rho_\alpha(r)\cos^4\phi + (1-\rho_\alpha(r))(8/15)\right] \nu_i^2(r,0) \qquad (16)$$

where $\nu_i^2(r,0)$ is the backscatter power ratio for a drop viewed at horizontal incidence and the relation $\nu_i(r,\phi) = \nu_i(r,0)\cos^2\phi$ is assumed. The factor 8/15 results from integrating $\cos^4\phi$ over all orientations. Alternately, we can calculate the quantity $\nu_i^2(r,\phi)$ directly from the scattering amplitude coefficients. Using this procedure, we compute the power ratio by the formula

$$\nu^2(r,\phi) = \rho_\alpha(r)\nu_i^2(r,\phi) + (1-\rho_\alpha(r))\ (8/15)\ \nu_i^2(r,0) \qquad (17)$$

The power ratio $\nu_i^2(r,0)$ calculated from the scattering amplitude coefficients of Oguchi and Hosoya is shown in Figure 2 for two wavelengths as a function of fall speed V(r) which was calculated from the formula of Best (1950). While one could not obtain this curve from actual observations at zero elevation angle, because the Doppler velocity component due to fall speed is proportional to $\sin\phi$, one could obtain an approximation to the curve by plotting $(S_1/S_2)/\cos^4\phi$ against $v/\sin\phi$. The result would be identical to Figure 2 in the ideal case of a completely oriented medium with zero air velocity. Non-zero air velocity would result in a displacement along the abscissa. Propagation effects and air velocity variance result in changes which are discussed and illustrated in Section III.

D. Computational Parameters and Procedures

Our model requires as input parameters the rainfall rate, air velocity standard deviation Σ, radar elevation angle ϕ, preferential orientation factor ρ_α, and propagation distance. For calculations based on Rayleigh scattering, we can use any values of these parameters (except propagation distance, which is not included in this case) since the scattering cross-section, power and amplitude ratios, and drop size distribution are defined by analytic functions. For calculations based on Mie scattering, we use the scattering amplitude coefficients and rates of differential attenuation (dB km^{-1}) and differential phase shift (deg km^{-1}) from Oguchi and Hosoya. Consequently, in this case, we are restricted to the elevation angles for which the amplitude coefficients were calculated (0^o, 20^o, 40^o, and 60^o) and the rainfall rates for which ΔA and $\Delta\Phi$

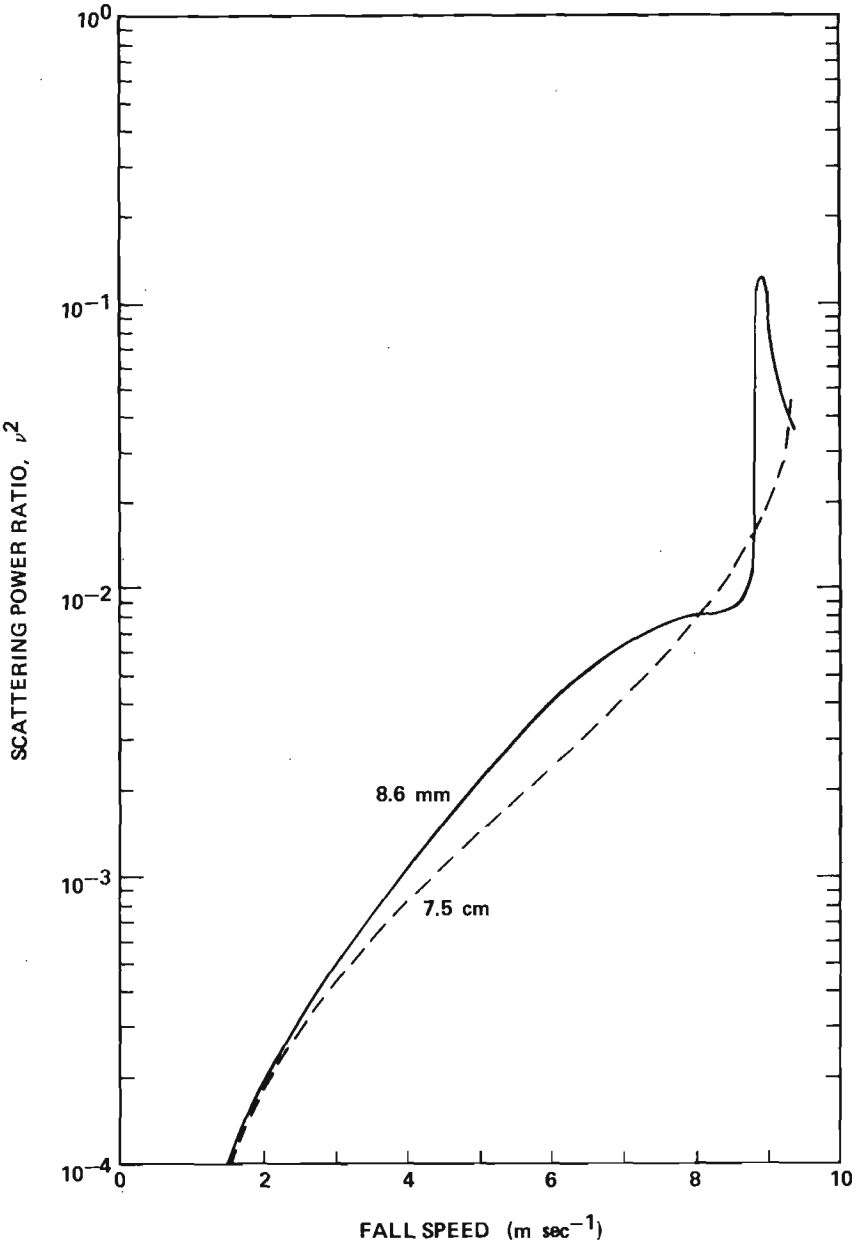

Figure 2. Scattering power ratio at zero elevation angle as a function of raindrop fall speed for radar wavelengths of 7.5 cm and 8.6 mm, based on the calculations shown in Figure 1. Power ratio for 8.6 mm shows sharp increase near 8.8 m sec^{-1} fall speed, corresponding to drops of diameter near 4.3 mm.

were calculated (0.25, 1.25, 2.5, 12.5, 25, 50, 100, and 150 mm hr^{-1}). We use the Marshall and Palmer raindrop size distribution function and the fall speed formula of Best. For simplicity, we assume $\bar{\alpha} = \tau = 0$.

We calculate the term pe^{jX} for the specified propagation distance. We then calculate three integral quantities at intervals of 0.1 m sec^{-1} between -2 and 16 m sec^{-1}:

$$I_1(v)=\int_{r_{min}}^{r_{max}} \sigma(r,\phi)\ N(r)\ G(V(r)\sin\phi,\Sigma)\ dr \tag{18}$$

$$I_2(v)=\int_{r_{min}}^{r_{max}} \sigma(r,\phi)\ N(r)\ G(V(r)\sin\phi,\Sigma)$$

$$\times \left[\rho_\alpha v_i^2(r,\phi)+(1-\rho_\alpha)\ \frac{8}{15}\ v_i^2(r,0)\right] dr \tag{19}$$

$$I_3(v)=\rho_\alpha\int_{r_{min}}^{r_{max}}\sigma(r,\phi)\ N(r)\ G(V(r)\sin\phi,\Sigma)v_i(r,\phi)e^{j\delta_i(r,\phi)}dr \tag{20}$$

We use r_{min}=0.1 mm, r_{max}=3.25 mm, and $\Delta r = 3.15\times10^{-3}$ mm, interpolating the scattering coefficients linearly between the radii at which they were calculated.

The power spectra and cross-spectrum are then calculated as follows:

$$S_1(v) = I_2(v)+4p^2 I_1(v)+4\mathrm{Re}\left[pe^{-jX}I_3(v)\right] \tag{21}$$

$$S_2(v) \equiv I_1(v) \tag{22}$$

$$S_{12}(v) = I_3(v) + 2pe^{jX}I_1(v) \tag{23}$$

The secondary spectral functions S_1/S_2 and S_{12}/S_2 are formed from these in accordance with Equations (9) and (10). We integrate the three primary spectral functions to obtain an approximation of the total reflectivity as defined in Equation (6), the circular

depolarization ratio, the cross-covariance and cross-correlation, and the Doppler velocity mean and standard deviation in each channel.

We have included the option of inserting a uniform "noise" spectral density at a specified decibel level below the peak of the spectrum S_2. This corresponds to radar system noise with a Delta function autocorrelation and zero cross-correlation between the noise and the signal. The noise spectral density is added to S_1 and S_2 across the Doppler velocity domain. If the noise in each channel is uncorrelated with the signal and with the noise in the other channel, then the presence of noise in the received signals has no effect on the cross spectrum S_{12}. There is, however, a significant effect on the spectral power ratio S_1/S_2 and on the modified cross-spectrum S_{12}/S_2, as illustrated in Section III.

Output options include plots and listings of the two power spectra, real and imaginary parts of the cross-spectrum, the spectral power ratio S_1/S_2, real and imaginary parts of S_{12}/S_2, and magnitude and phase of S_{12}/S_2 as functions of Doppler velocity v. In addition, one can plot the function S_{12}/S_2 in the complex plane with points designated at specified velocity values, typically each 1 m sec^{-1}.

These computations and output procedures were programmed in FORTRAN for the Digital Equipment Corporation VAX-11/780 computer and California Computer Products CALCOMP 1012 plotter operated by the Radar and Instrumentation Laboratory in the Engineering Experiment Station. The VAX has absolute numerical limits of 10^{-38} and 10^{38}, which necessitate the substitution of zero for spectral density values that would be less than 10^{-38}. This consideration accounts for some apparently anomalous features on some of the plots. The numerical limits also introduce difficulty in the computation of ratios of very small numbers or very large numbers. Numerical accuracy of the results is also affected by the procedures we used, including the trapezoid-rule integration, the radius limits, and the linear interpolation of the scattering coefficients.

III. RESULTS

Our initial objective was to determine the effects of variations in parameters on the resulting spectral functions. Hence, we have run the model calculations to generate sets of functions corresponding to variations in turbulence intensity and variations in propagation distance. We have endeavored to include in each of these sets one or more calculations with physically realistic values of the parameters. We have also used unrealistically large or small values of the parameters in order to explore asymptotic characteristics of some of the functions.

A. Turbulence Effects

Computations were performed with several values of air velocity standard deviation to illustrate the effects of air velocity fluctuation on the spectral functions and to attempt to generate functions approximating those shown in Figures 1 and 2. These are illustrated in Figures 3, 4, and 5 for 25 mm hr^{-1} rainfall rate and in Figures 6, 7, and 8 for 2.5 mm hr^{-1} rainfall rate. The spectra and power ratio computed with $\Sigma = 0.05$ and 0.1 show variations which are probably artifacts of the linear interpolation of the scattering coefficients, especially between 5 and 6 m sec^{-1} Doppler velocity. In this velocity region, the scattering characteristics change rapidly with Doppler velocity, since the raindrops producing these effects are falling within 70% to 85% of the maximum raindrop fall speed and the Doppler fall speed is changing slowly with drop size.

The effects of the numerical procedure with small values of Σ are more strikingly illustrated in the modified cross-spectrum S_{12}/S_2, shown in Figures 5a and 8a. Because of the rapid variation of drop size with fall speed for drops of 4 to 5 mm diameter, the rotation of the amplitude ratio shown in Figure 1 could only be duplicated if the spectral functions were computed at much smaller velocity intervals with correspondingly smaller values of Σ. The fact that this rapid rotation of the amplitude ratio vector occurs at lower Doppler velocities than would be expected from Figure 1 is difficult to explain; this is probably related to the weighting of the cross-spectrum by the backscatter cross-section and size distribution functions and to the irregularities of the cross-section function resulting from the linear interpolation. The spectral weighting effect is shown more distinctly in Figures 5b, c, and e and 8b, c, and e, with increasing

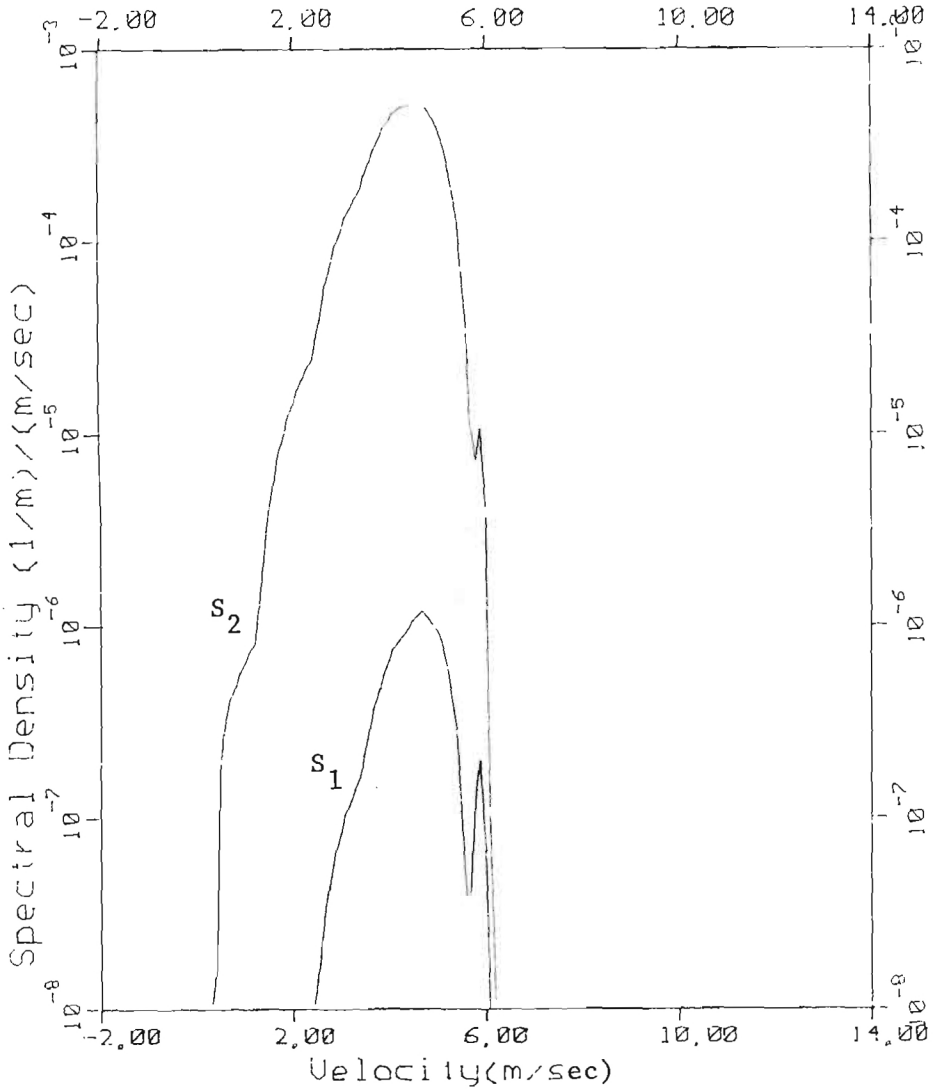

Figure 3a. Power spectra in transmission and orthogonal channels of circularly polarized 8.6-mm wavelength radar at 40^{0} elevation angle in 25 mm hr^{-1} rain, with $\Sigma = 0.05$ m sec^{-1}.

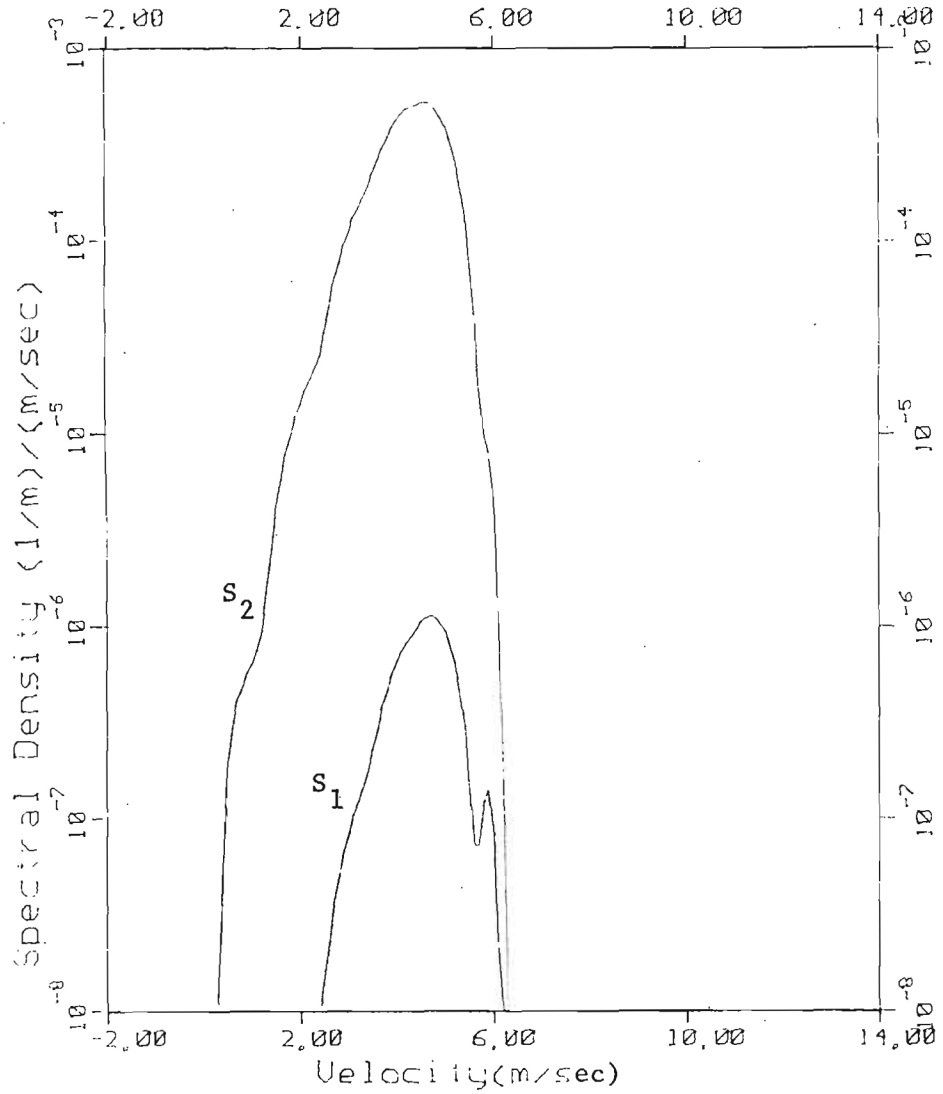

Figure 3b. Same as Figure 3a, with $\Sigma = 0.1$ m sec^{-1}.

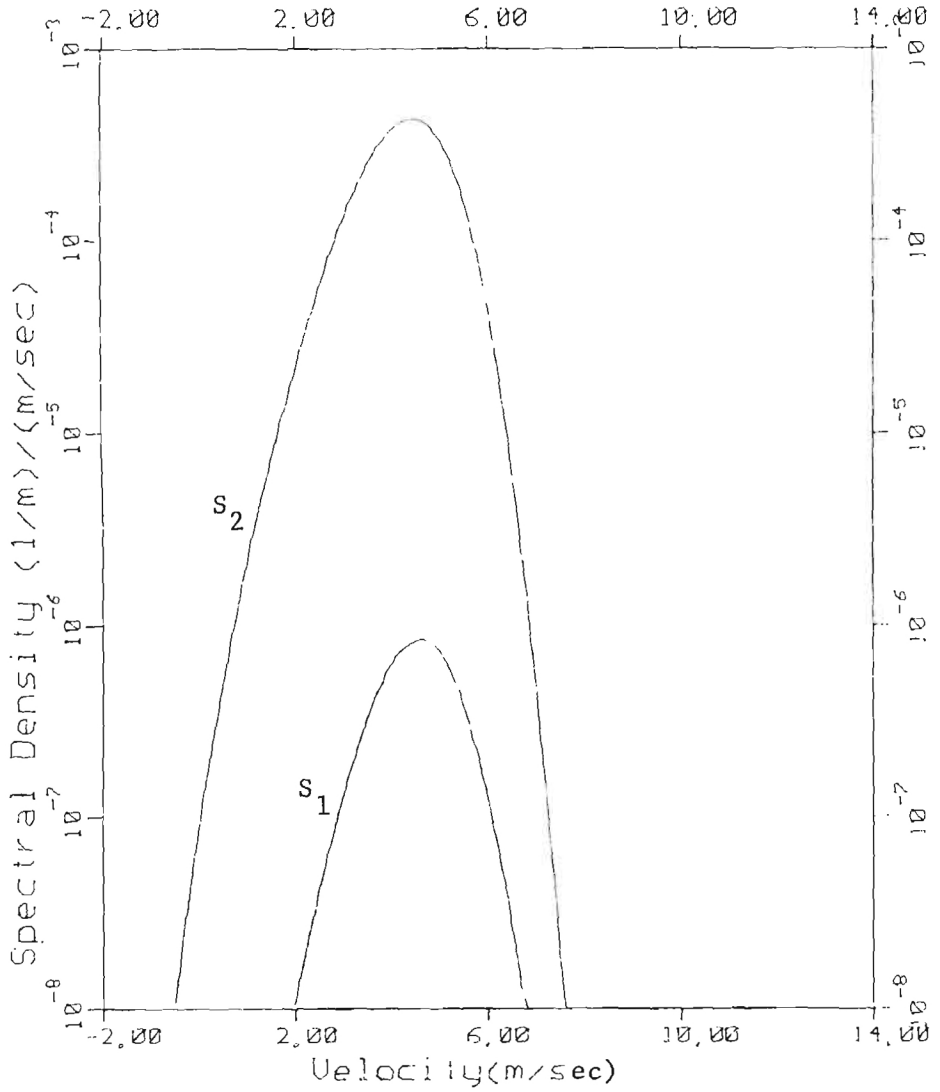

Figure 3c. Same as Figure 3a, with $\Sigma = 0.5$ m sec^{-1}.

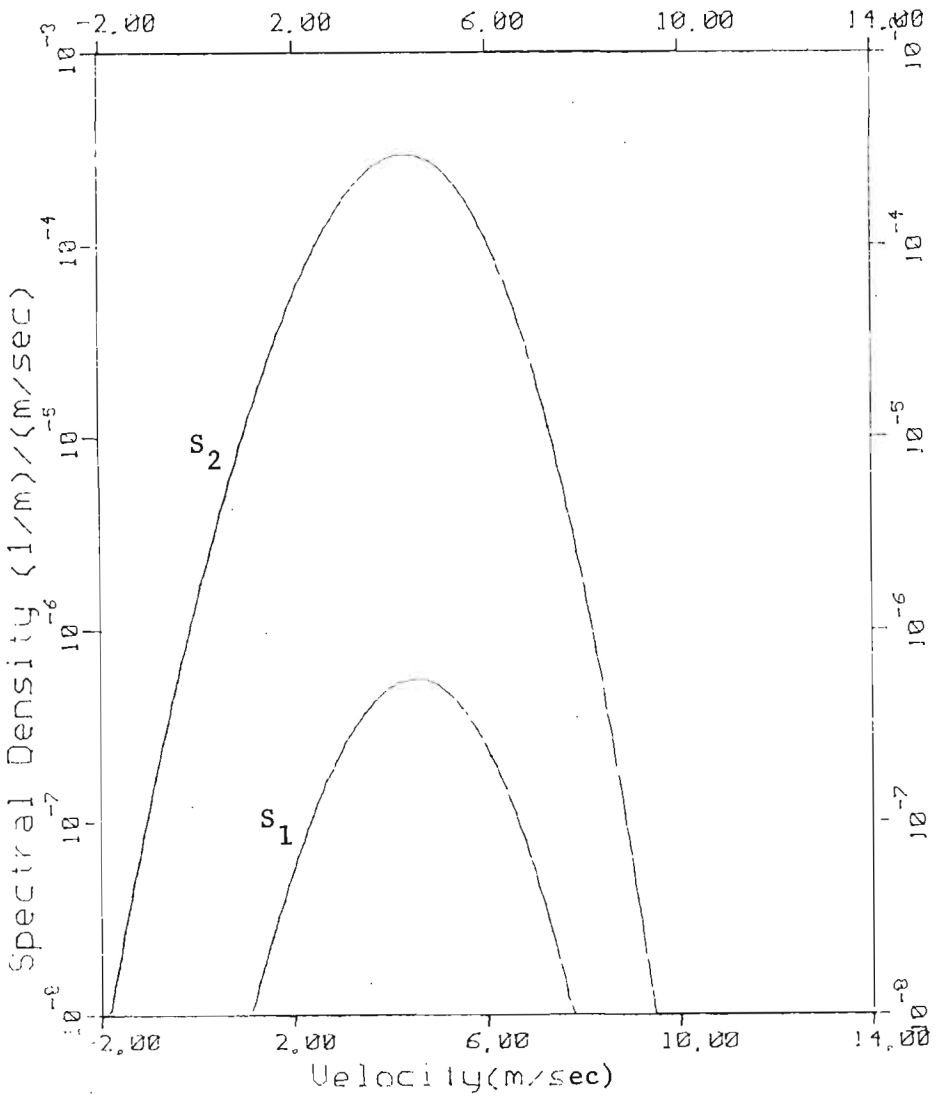

Figure 3d. Same as Figure 3a, with $\Sigma = 1.0$ m sec^{-1}.

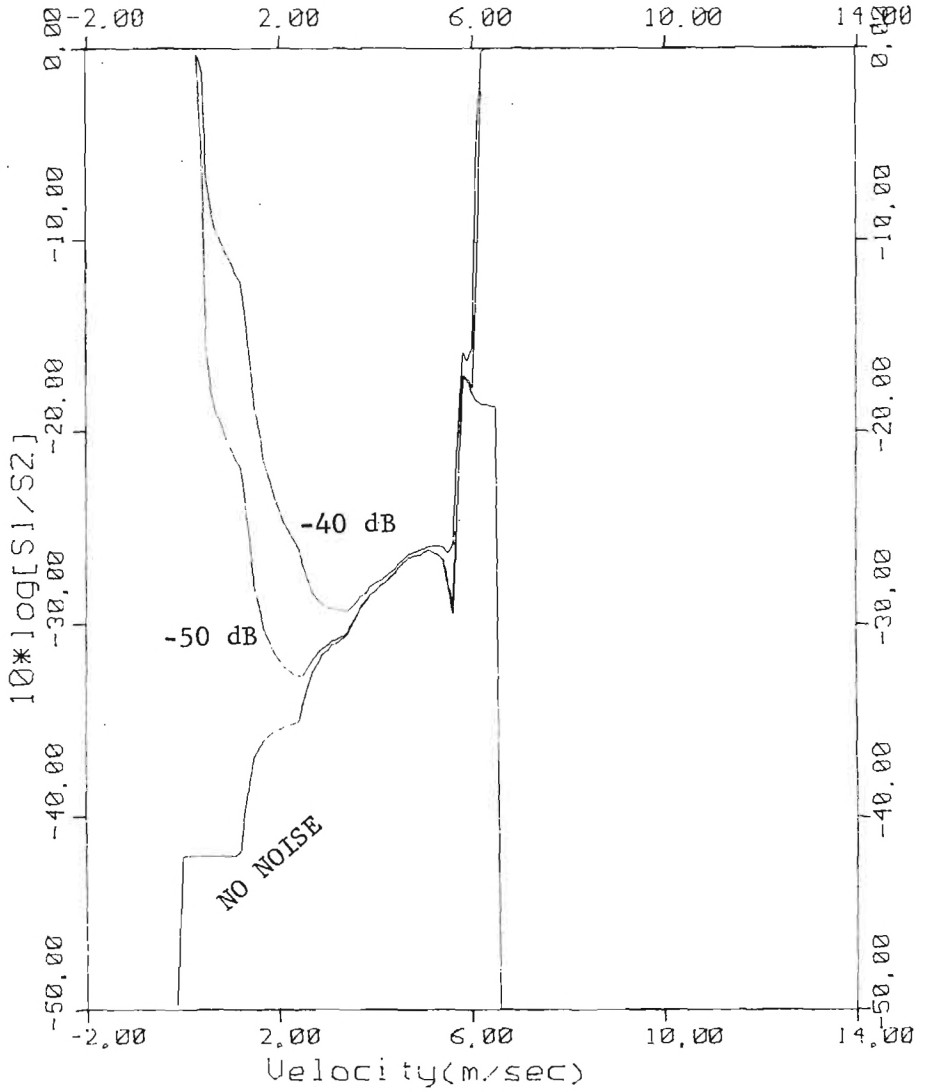

Figure 4a. Spectral power ratio for 40° elevation angle in 25 mm hr^{-1} rain, with Σ = 0.05 m sec^{-1} with no noise and with noise levels of 50 and 40 dB below the peak value of S_{21}. Apparent cutoffs of the noise-free case near zero and 6.5 m sec^{-1} Doppler velocity are due to numerical limits of the computations. In the presence of noise, the power ratio provides an estimate of the noise-free function over a limited velocity domain.

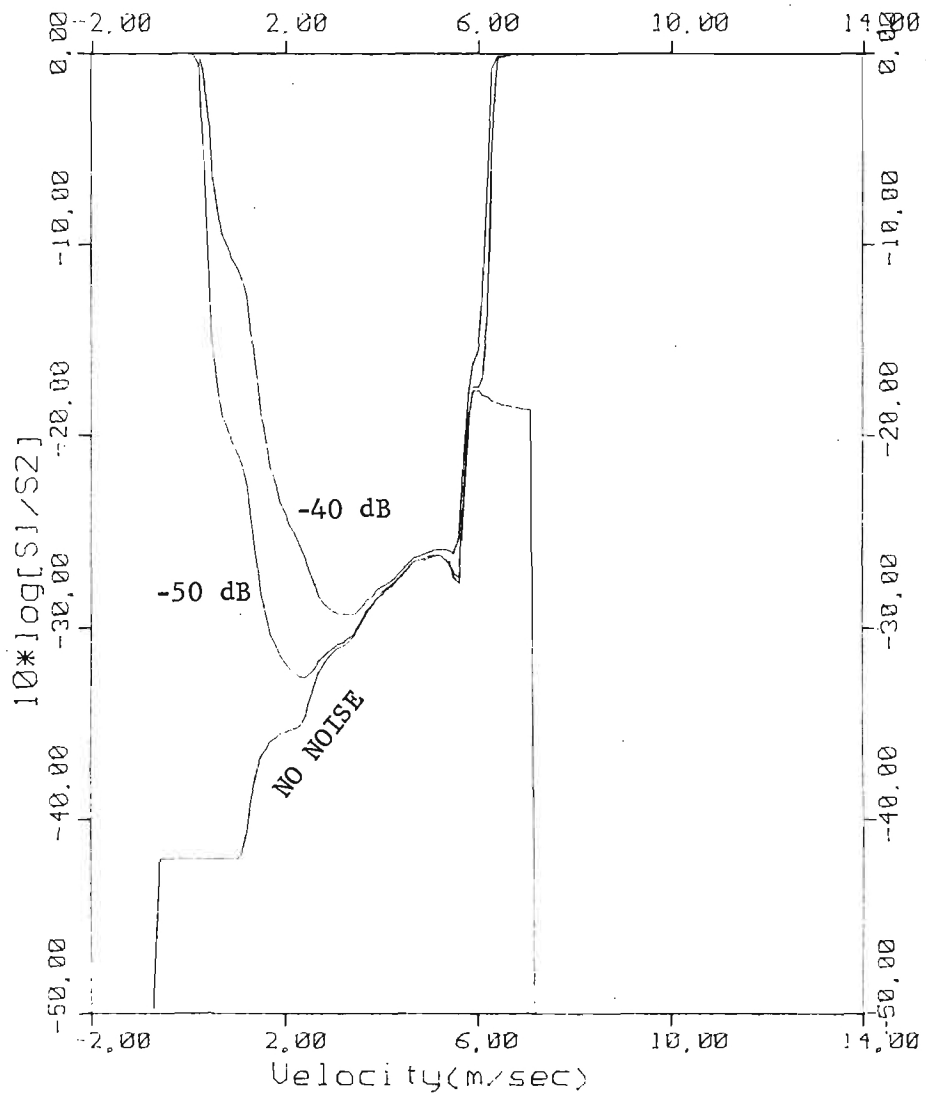

Figure 4b. Same as Figure 4a, with $\Sigma = 0.1$ m sec^{-1}.

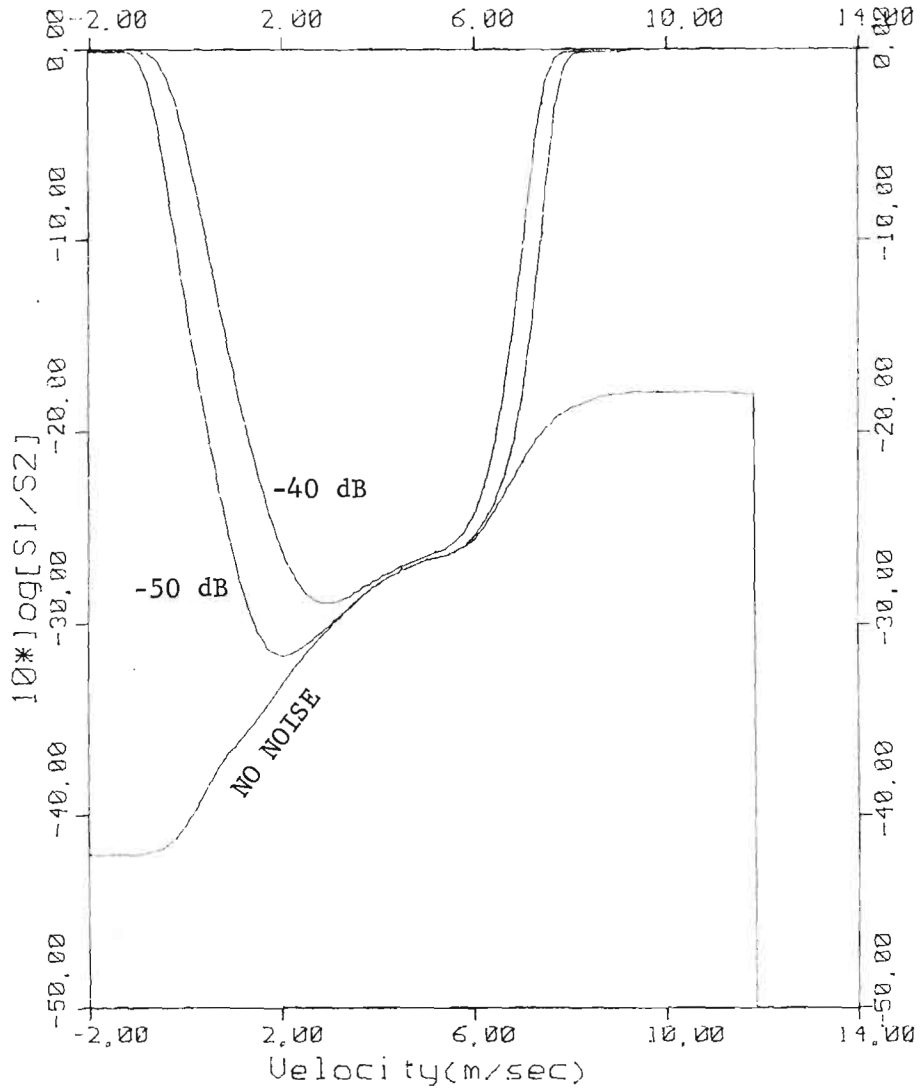

Figure 4c. Same as Figure 4a, with $\Sigma = 0.5$ m sec^{-1}.

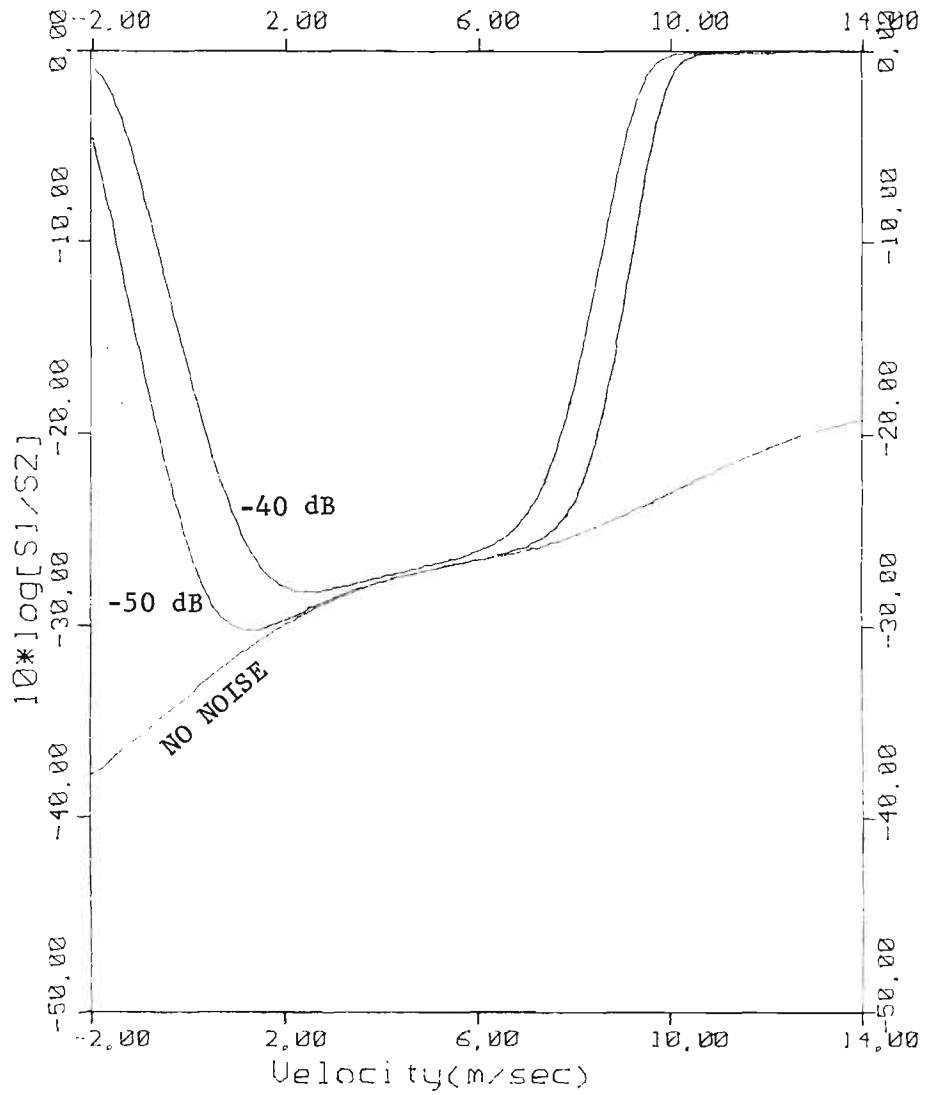

Figure 4d. Same as Figure 4a, with $\Sigma = 1.0$ m sec^{-1}.

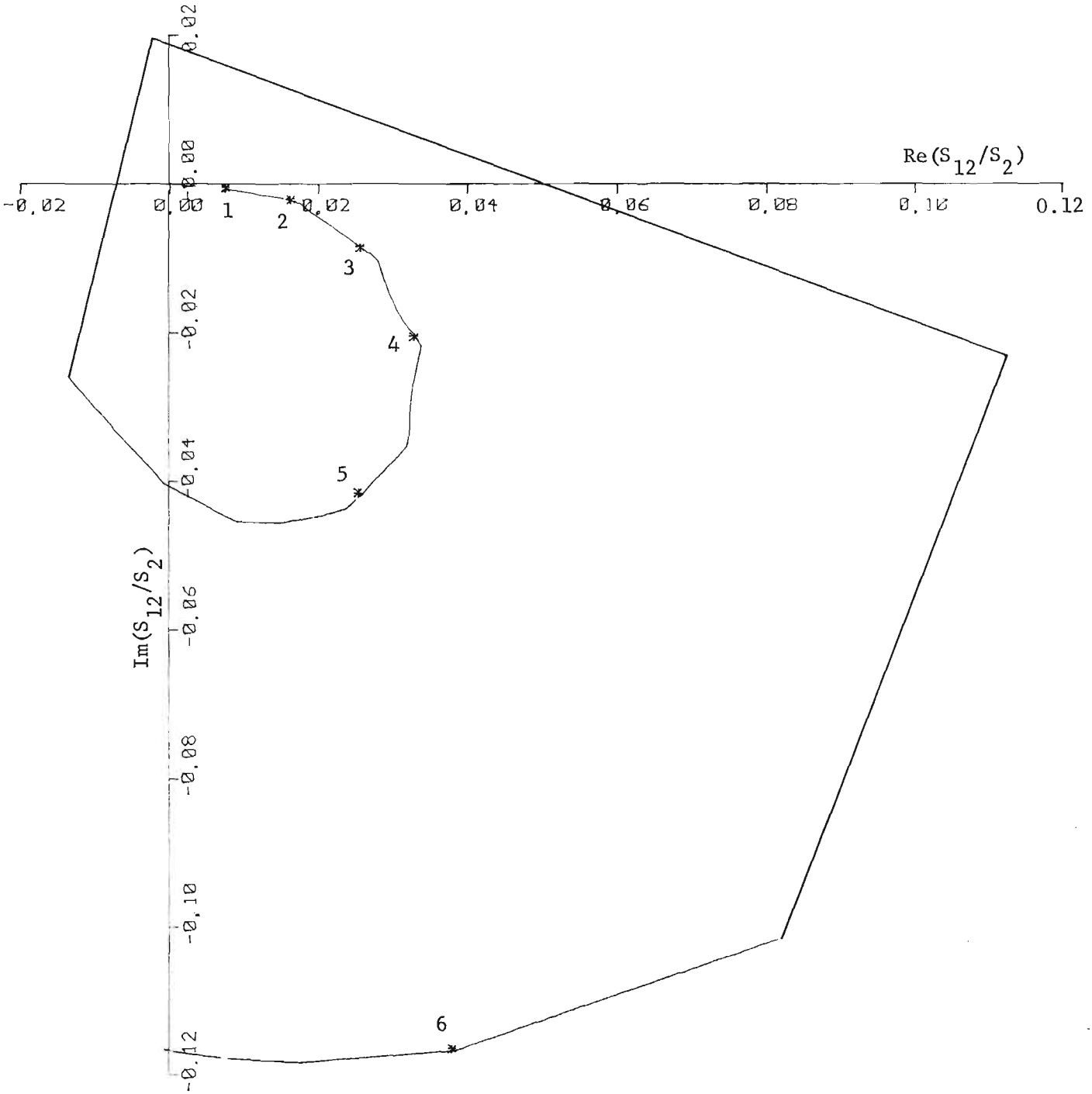

Figure 5a. Modified cross-spectrum for 40^{o} elevation angle in 25 mm hr^{-1} rain, with Σ = 0.05 m sec^{-1} and no noise. Segmented appearance of function beyond about 5.5 m sec^{-1} Doppler velocity is due to rapid variation of drop size and shape with Doppler fall speed in this region.

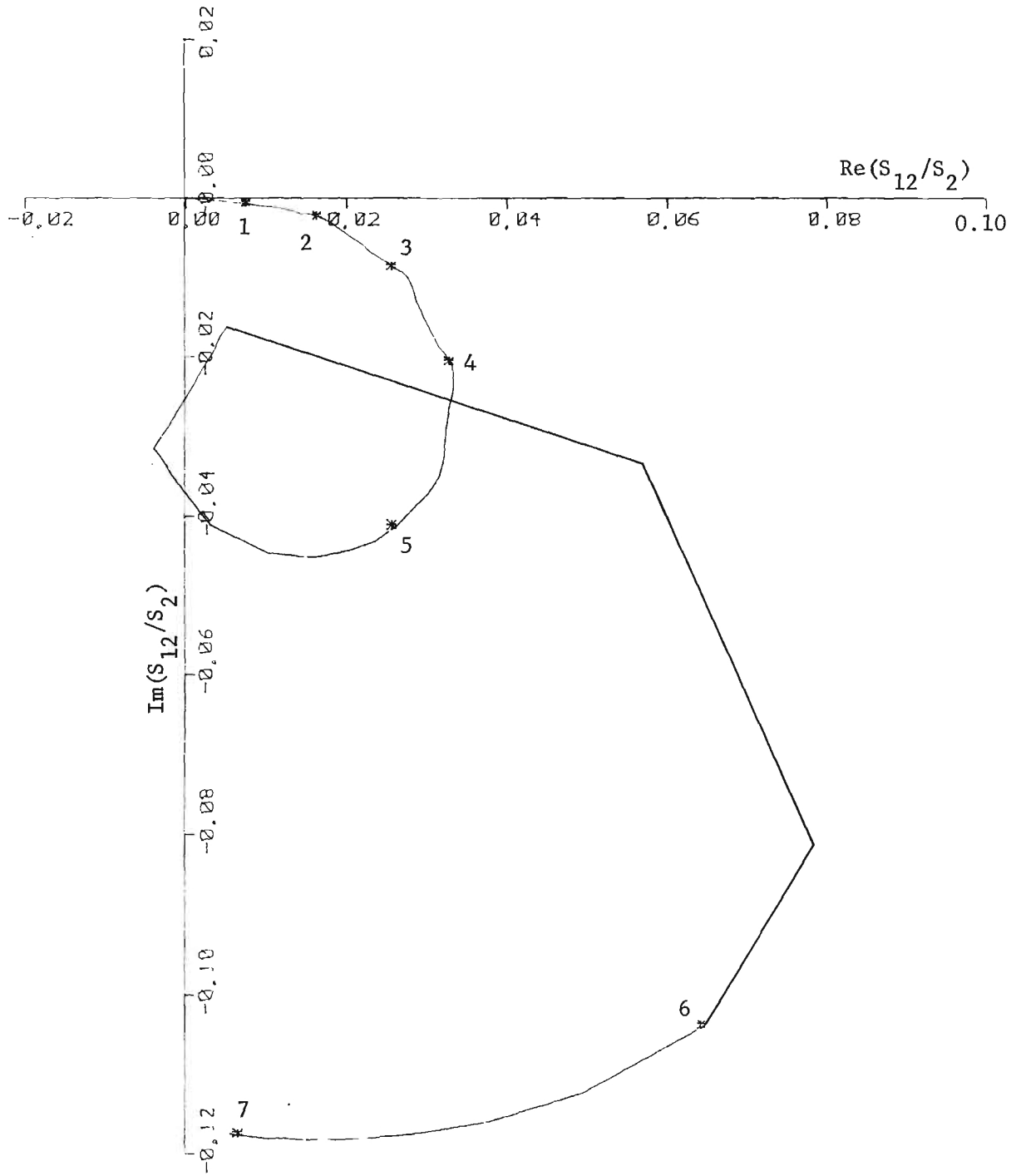

Figure 5b. Same as Figure 5a, with $\Sigma = 0.1$ m sec^{-1}.

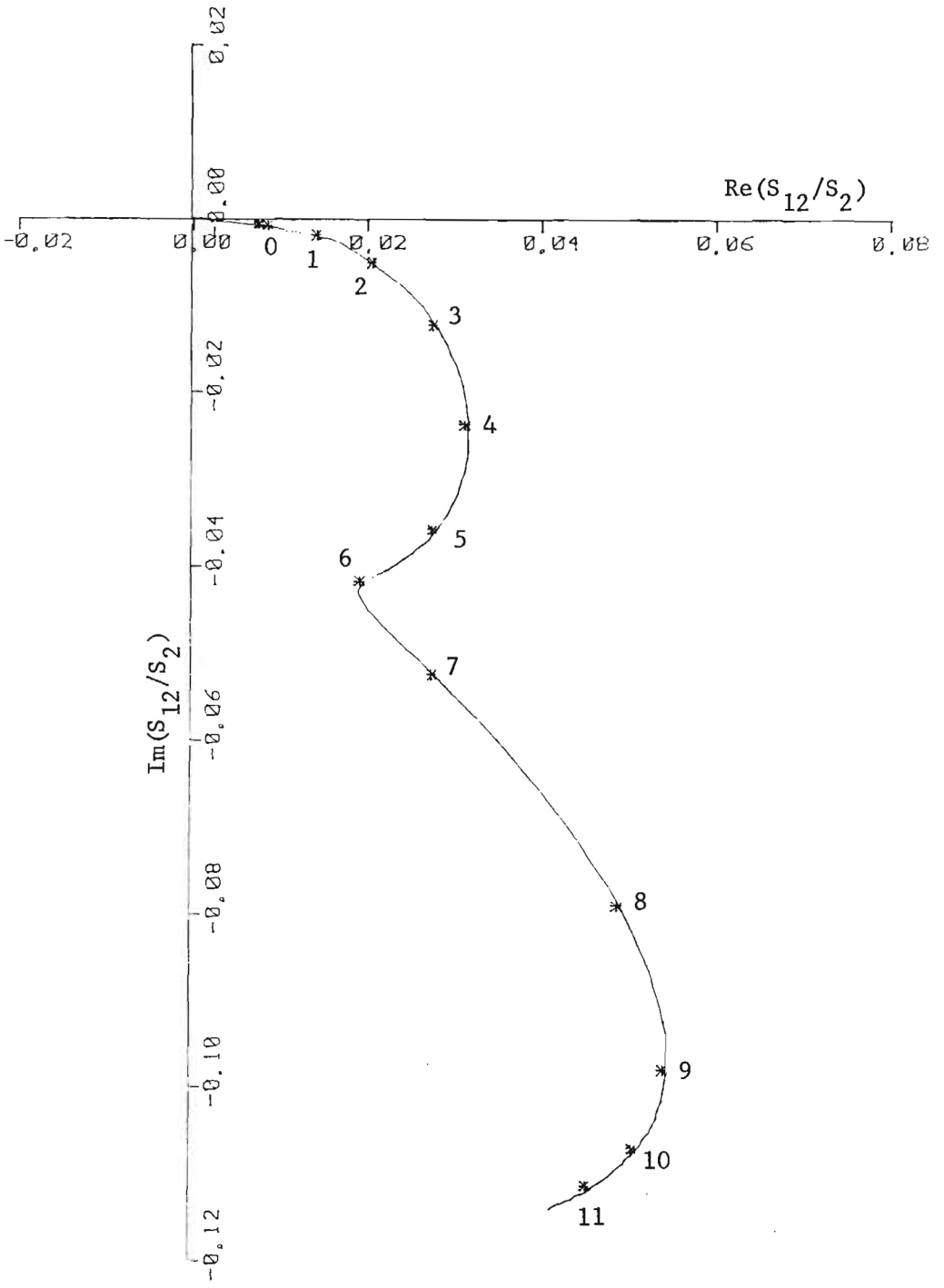

Figure 5c. Same as Figure 5a, with $\Sigma = 0.5$ m sec^{-1}. Smoothing due to increasing width of velocity weighting function is evident.

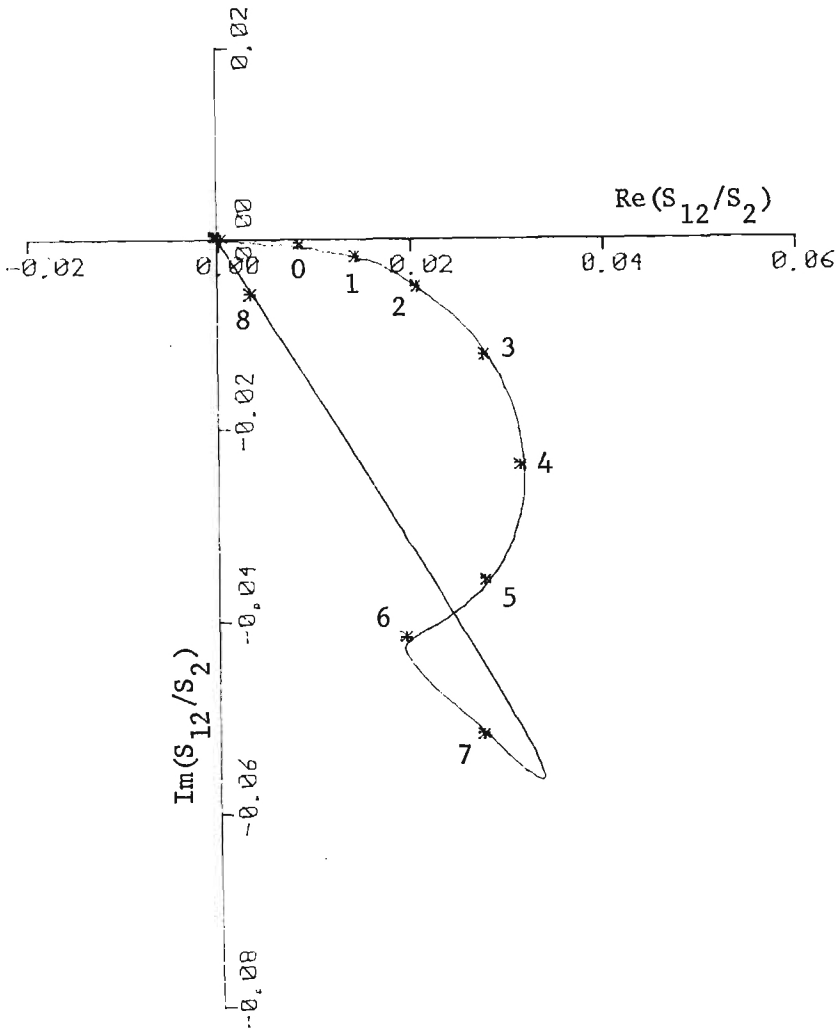

Figure 5d. Same as Figure 5c, with noise level of 50 dB below the peak of S_2. Minimum of the real part near 6 m sec^{-1} Doppler velocity is discernable at this noise level, but not with -40 dB noise.

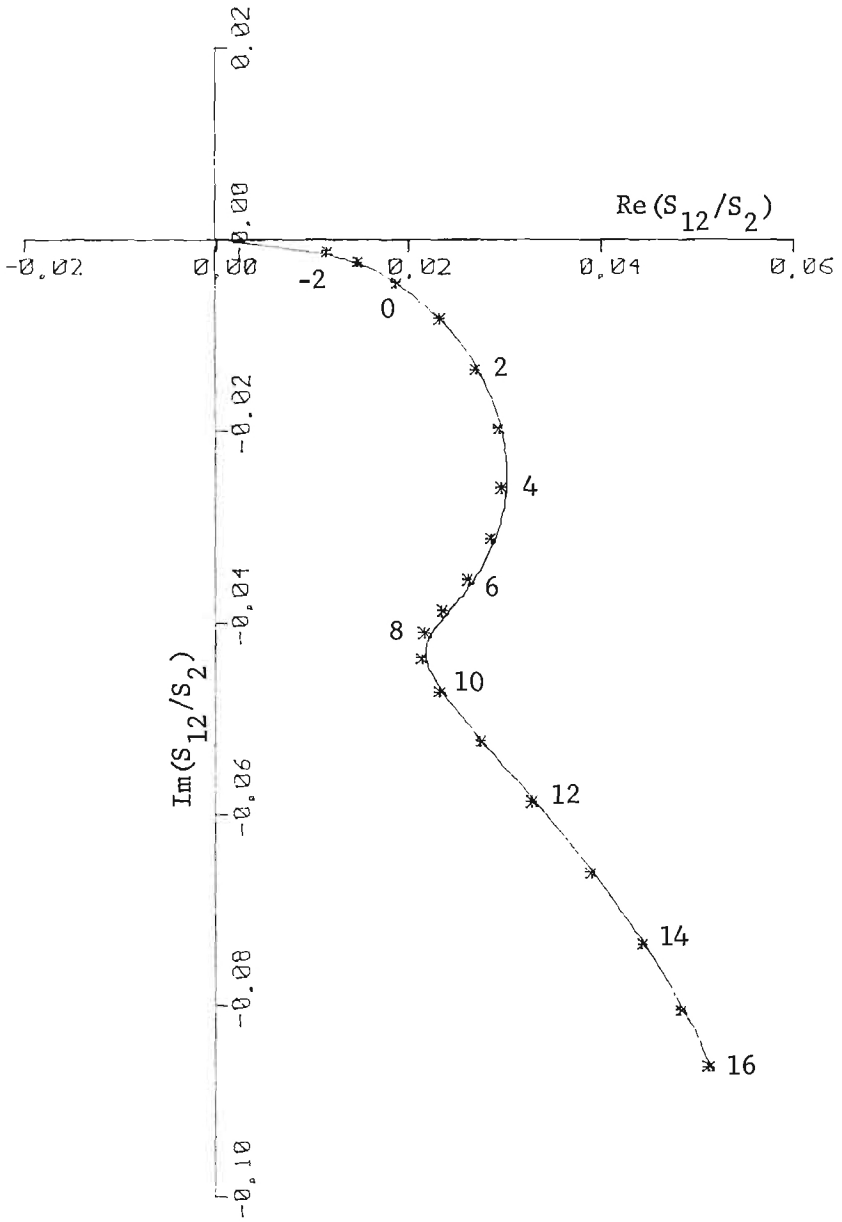

Figure 5e. Same as Figure 5a, with $\Sigma = 1.0$ m sec^{-1}.

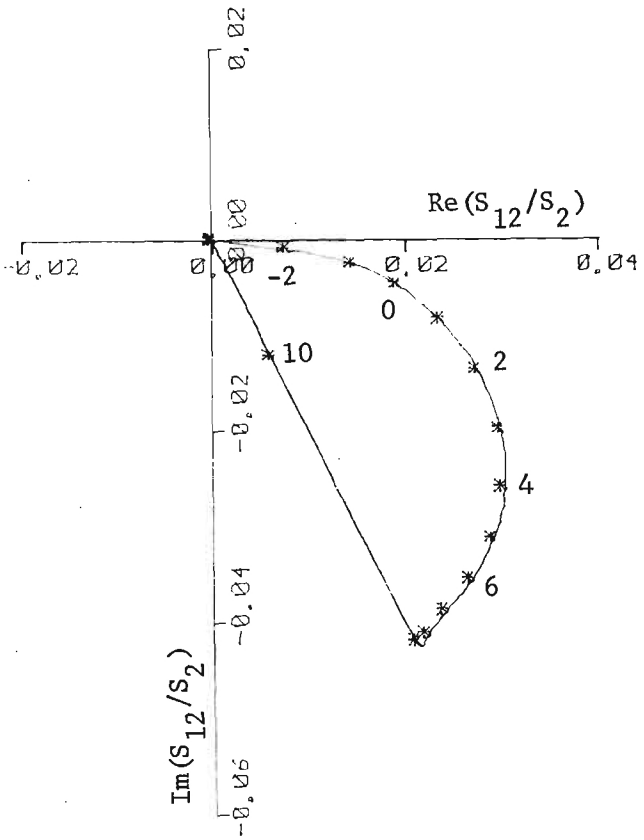

Figure 5f. Same as Figure 5e, with noise level of 50 dB below the peak of S_2. The minimum of the real part near 9 m sec^{-1} is not discernable in this case.

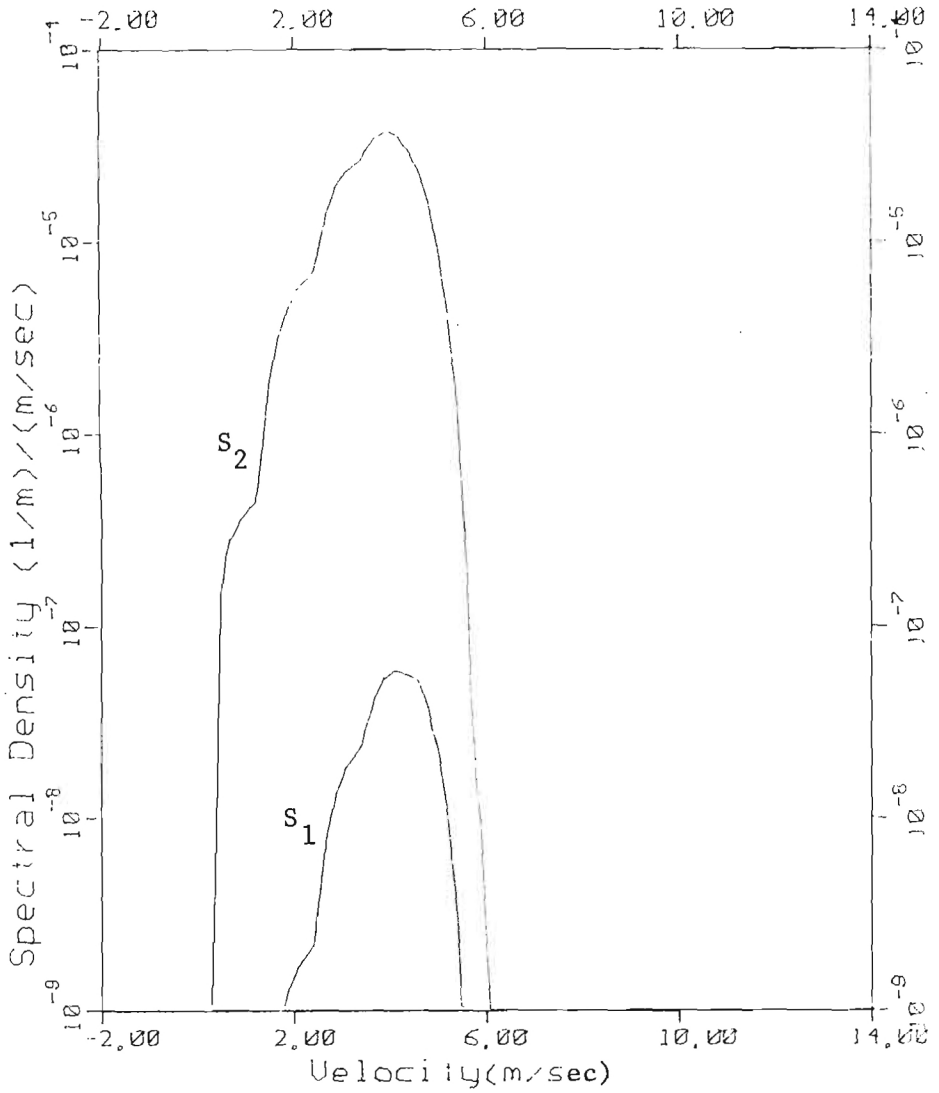

Figure 6a. Power spectra in transmission and orthogonal channels of circularly polarized 8.6-mm wavelength radar at 40^{0} elevation angle in 2.5 mm hr^{-1} rain, with $\Sigma = 0.05$ m sec^{-1}.

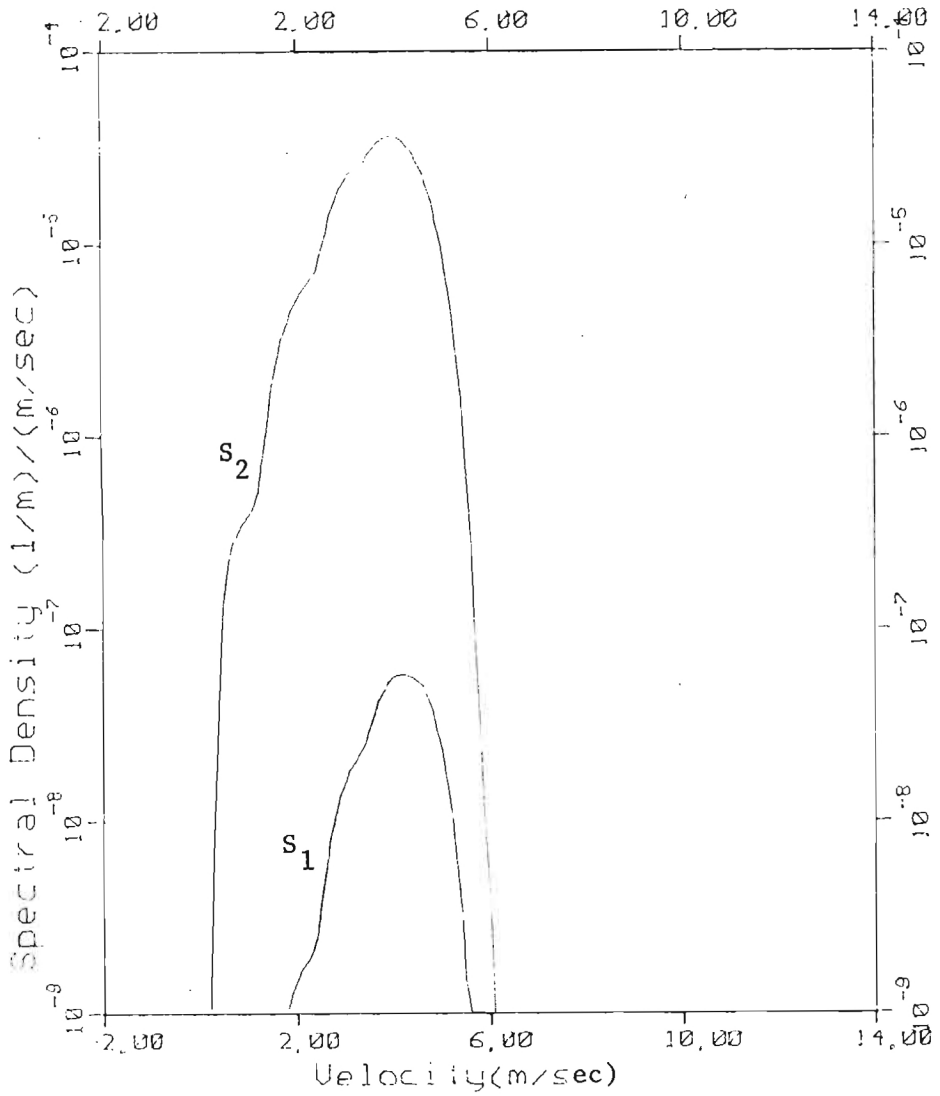

Figure 6b. Same as Figure 6a, with $\Sigma = 0.1$ m sec^{-1}.

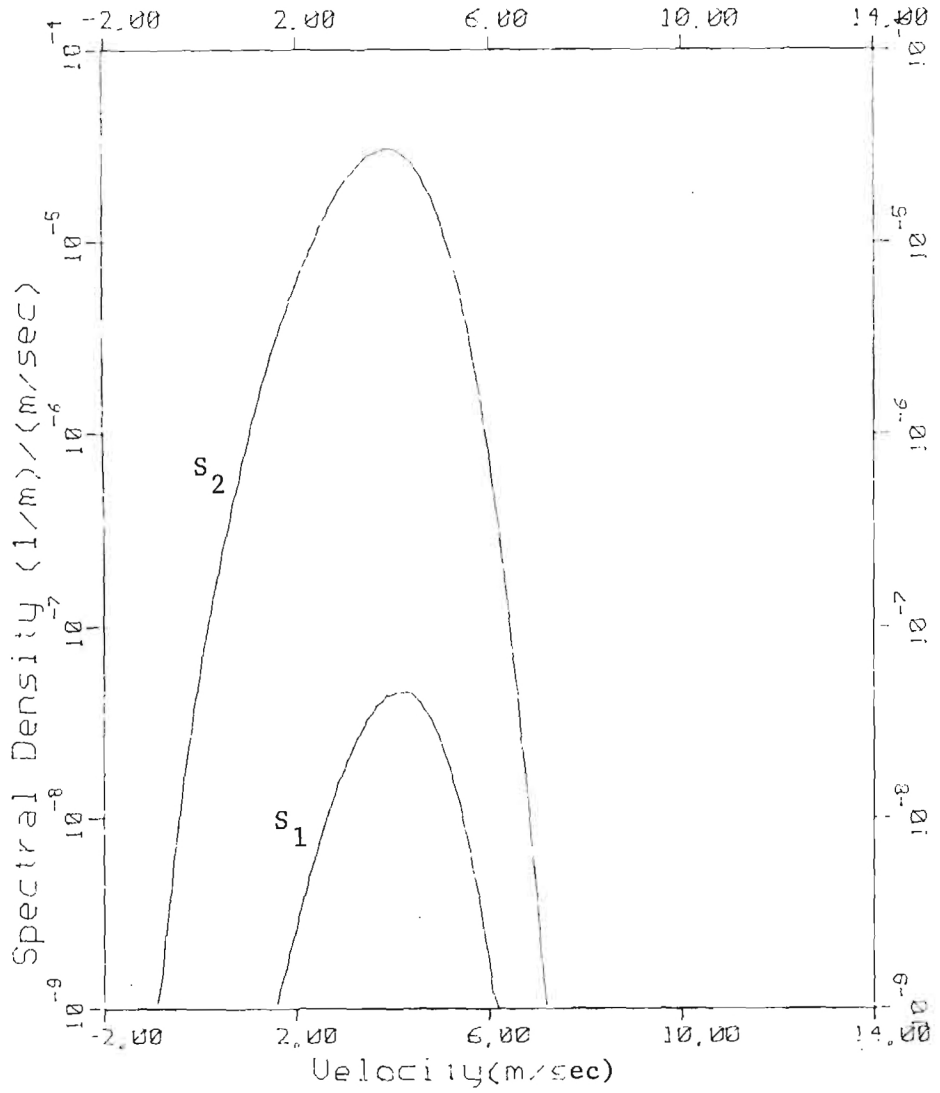

Figure 6c. Same as Figure 6a, with $\Sigma = 0.5$ m sec^{-1}.

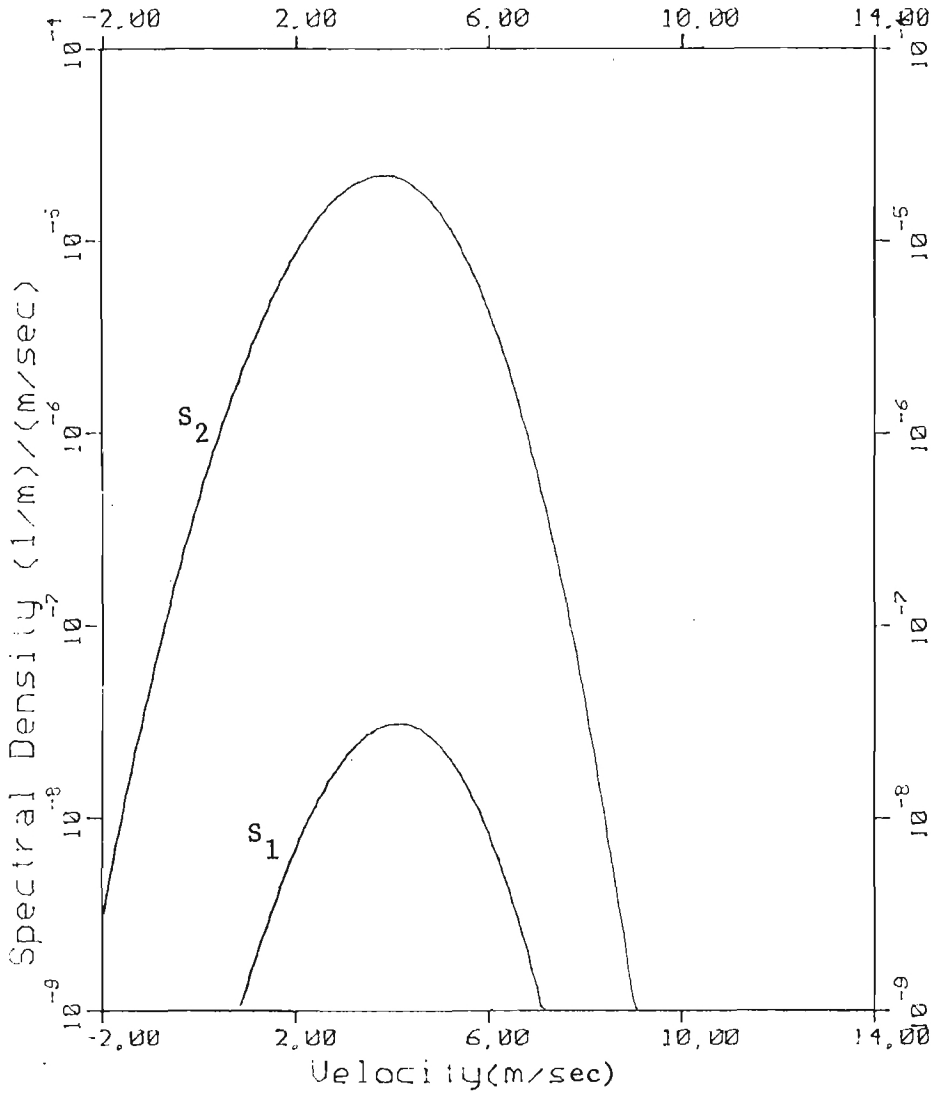

Figure 6d. Same as Figure 6a, with $\Sigma = 1.0$ m sec^{-1}.

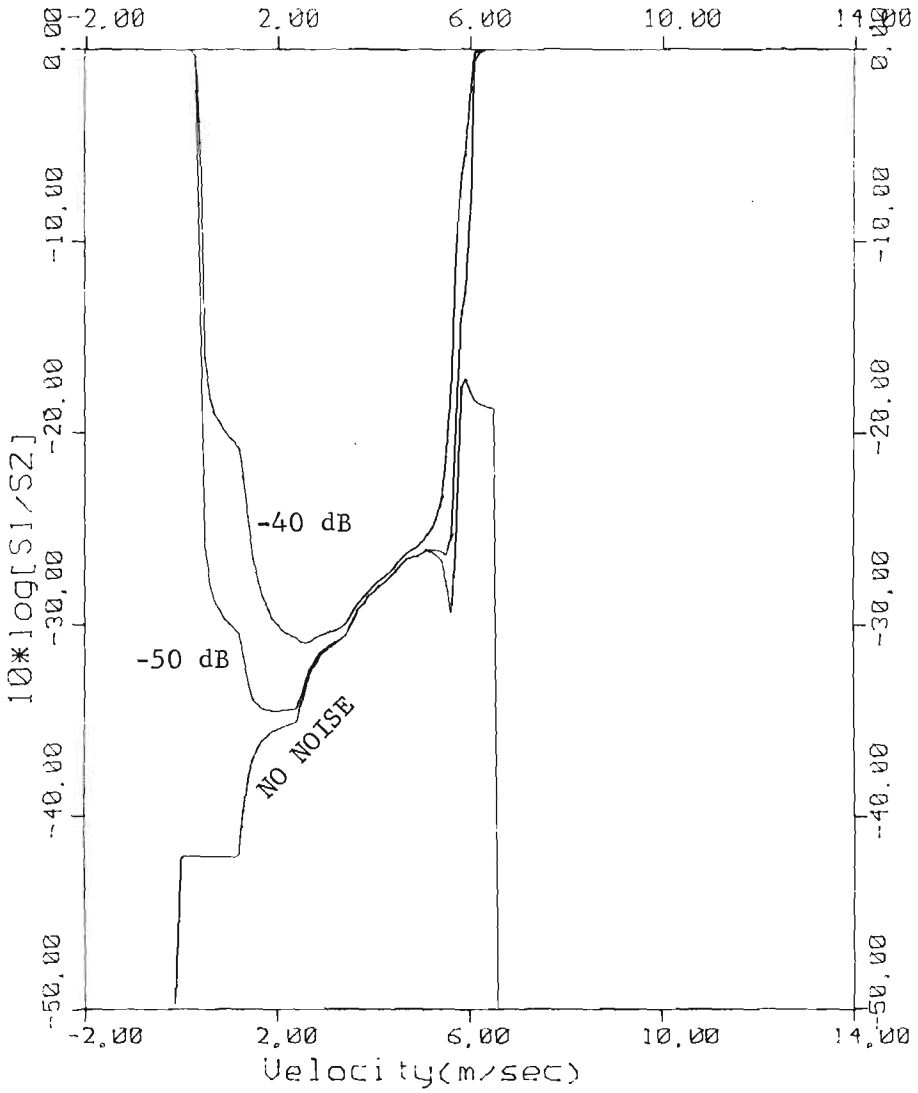

Figure 7a. Spectral power ratio for 40^{o} elevation angle in 2.5 mm hr^{-1} rain, with Σ = 0.05 m sec^{-1} with no noise and with noise levels of 50 and 40 dB below the peak of S_2.

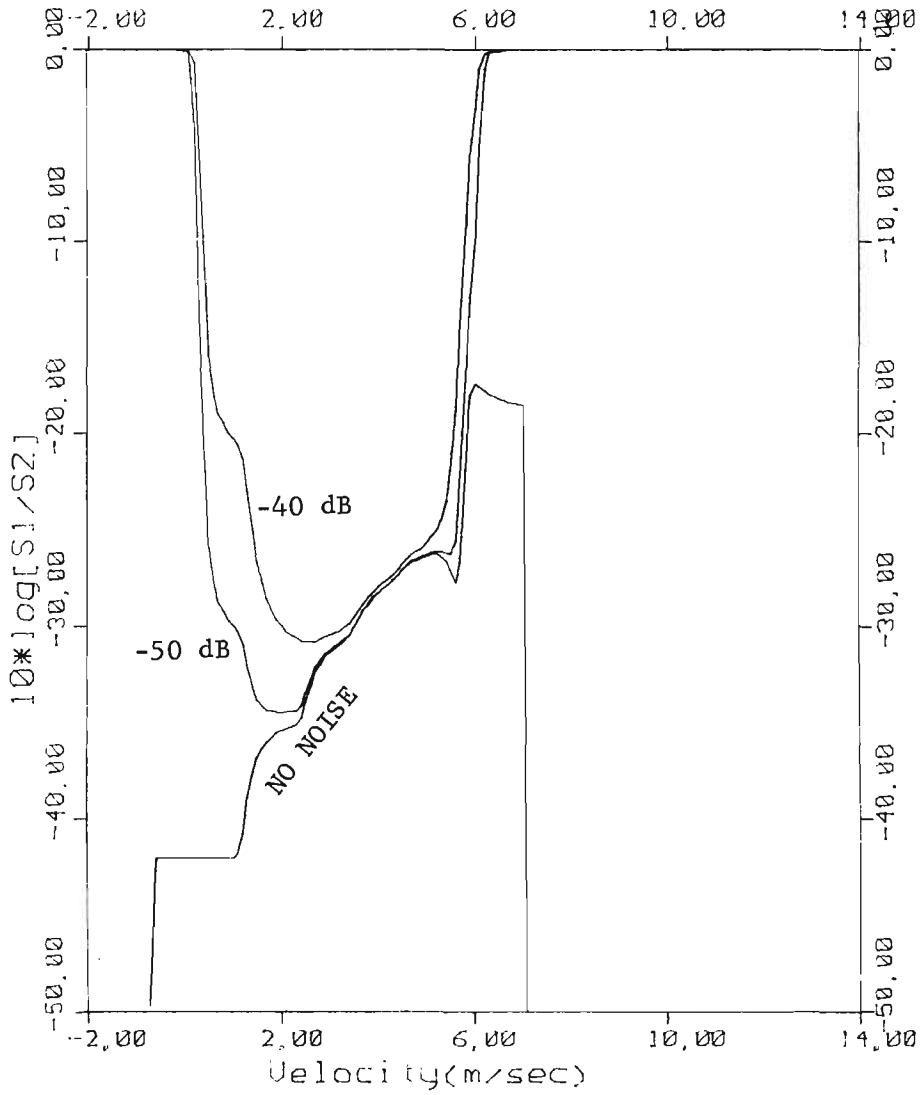

Figure 7b. Same as Figure 7a, with $\Sigma = 0.1$ m sec^{-1}.

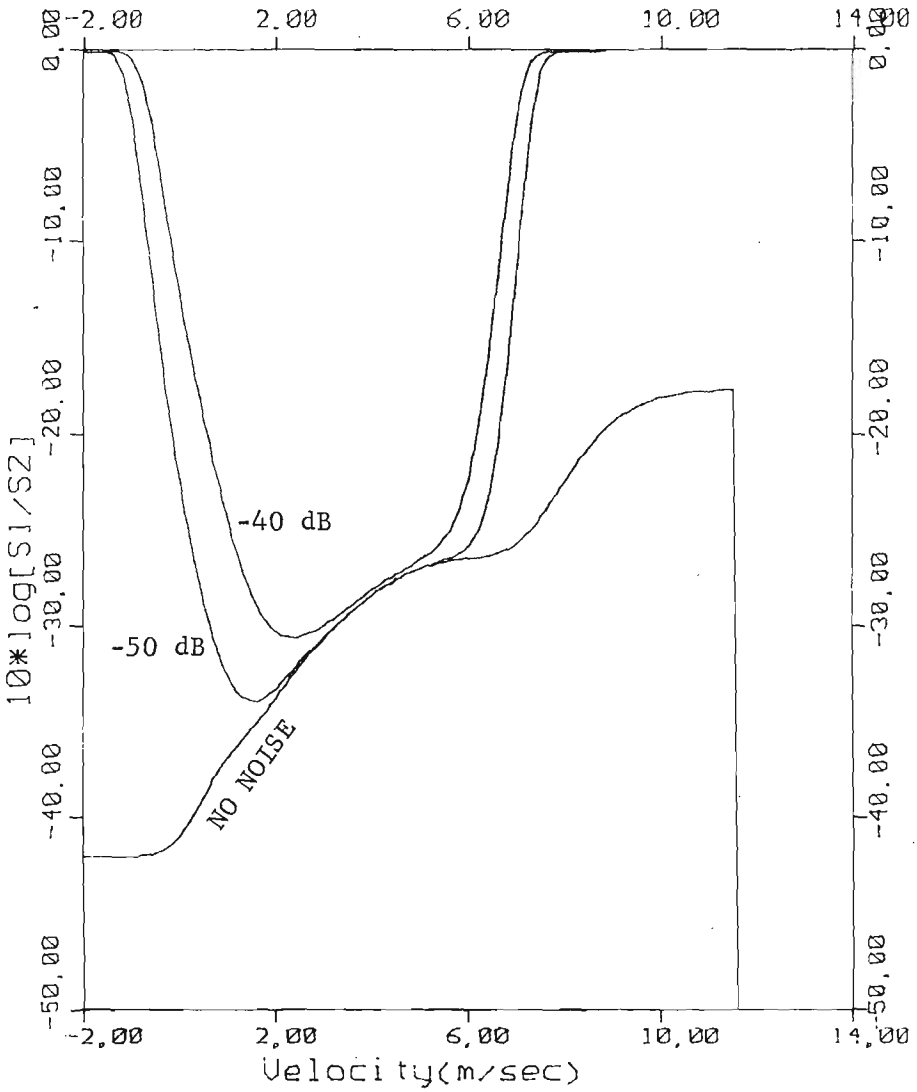

Figure 7c. Same as Figure 7a, with $\Sigma = 0.5$ m sec^{-1}.

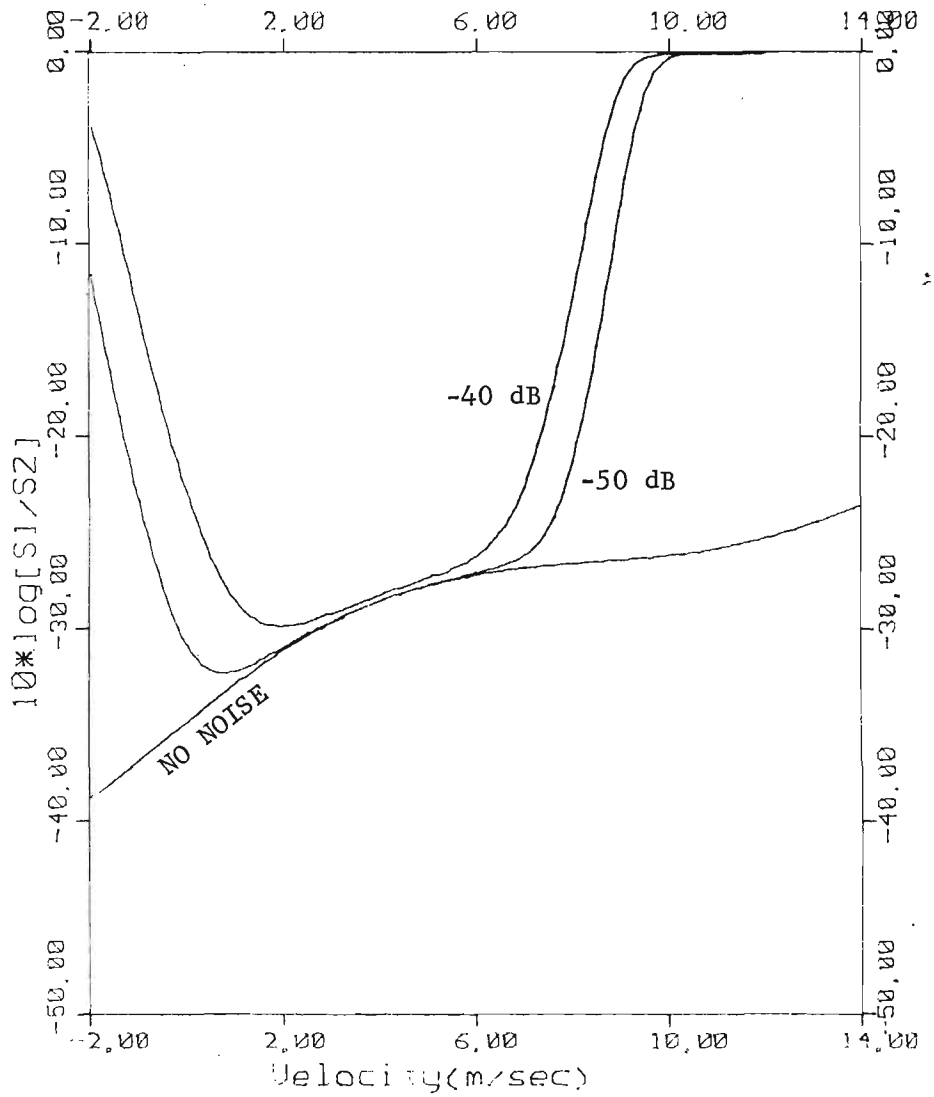

Figure 7d. Same as Figure 7a, with $\Sigma = 1.0$ m sec^{-1}.

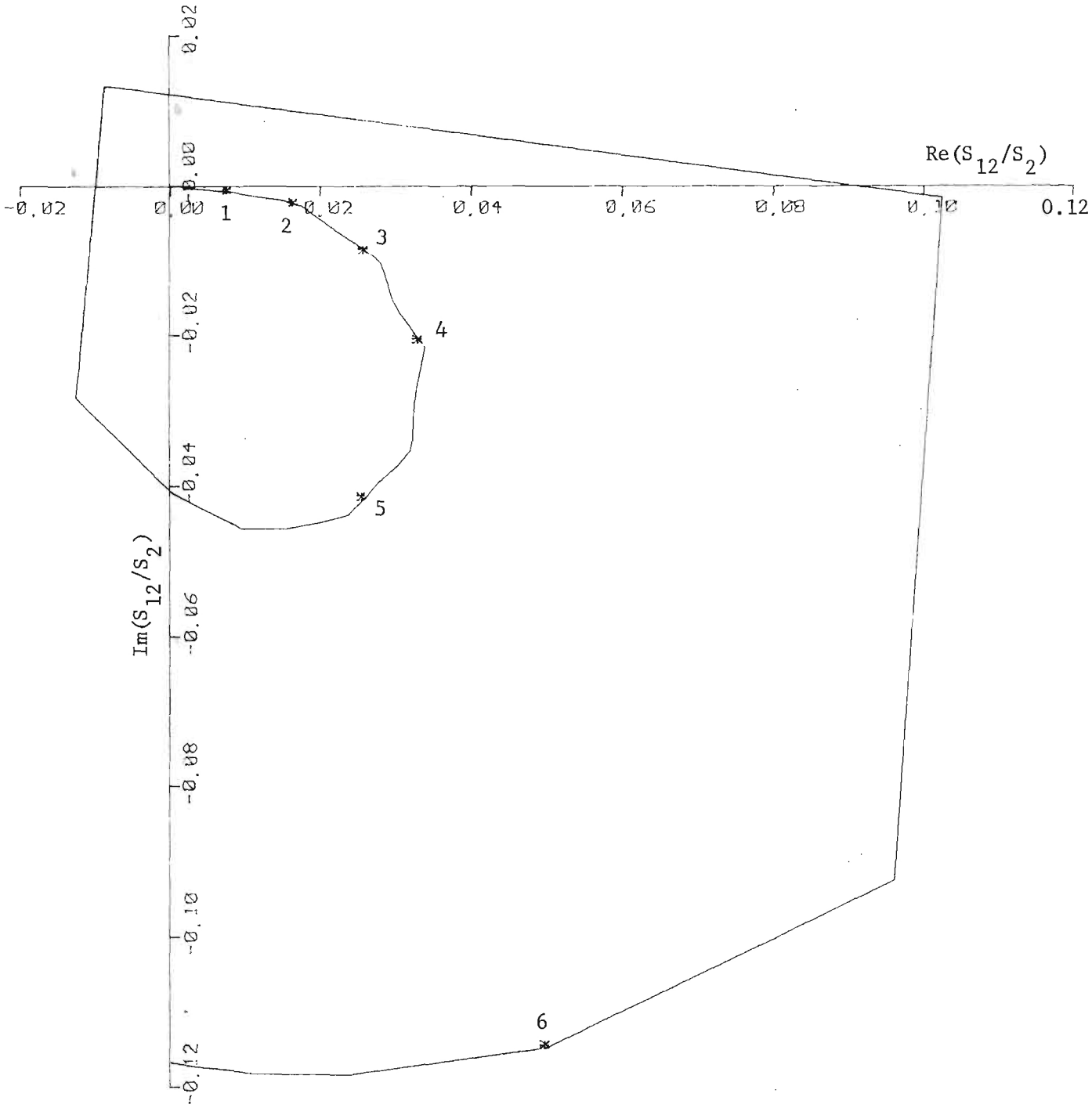

Figure 8a. Modified cross-spectrum for 40^{o} elevation angle in 2.5 mm hr^{-1} rain, with Σ = 0.05 m sec^{-1} and no noise.

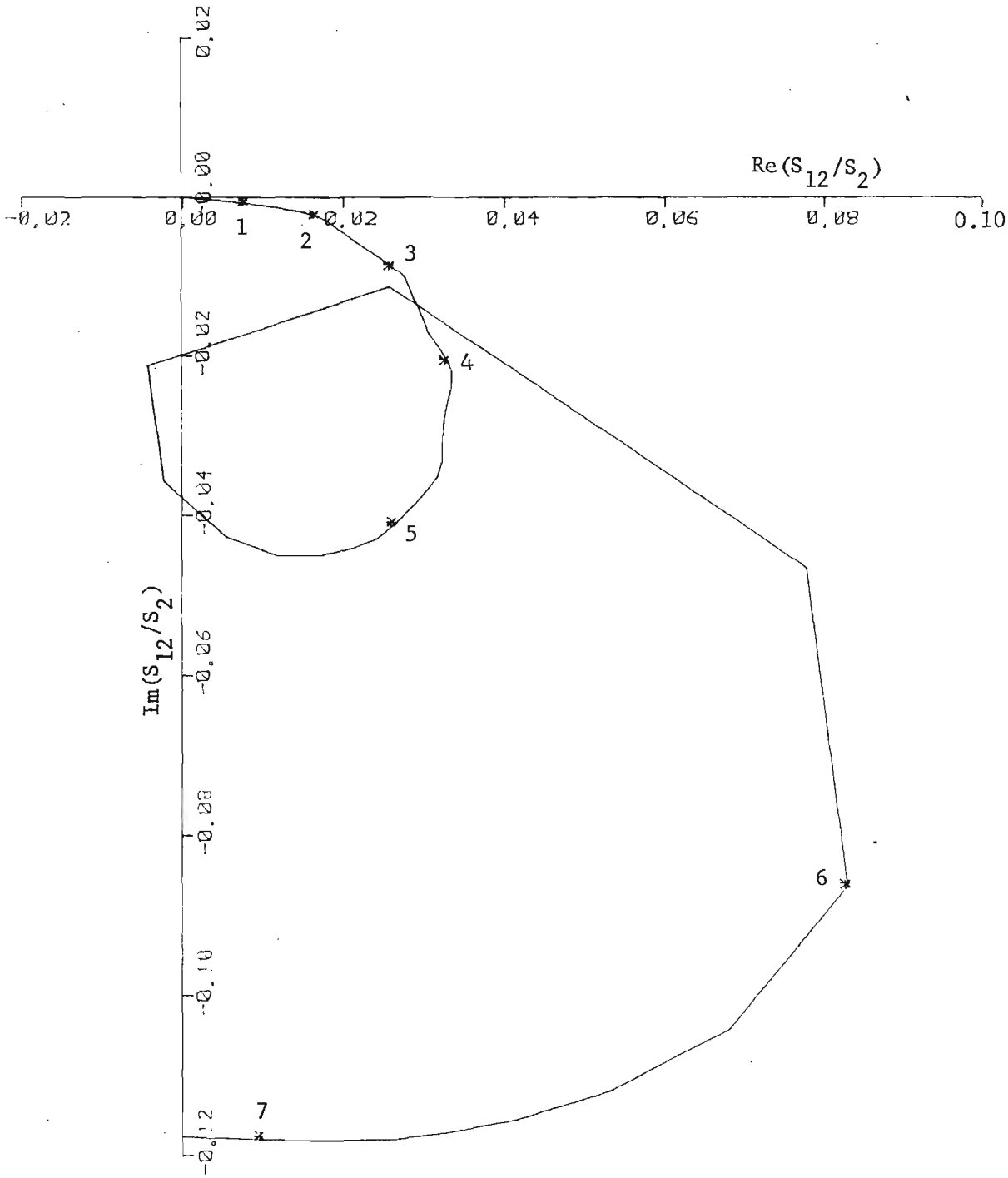

Figure 8b. Same as Figure 8a, with $\Sigma = 0.1$ m sec^{-1}.

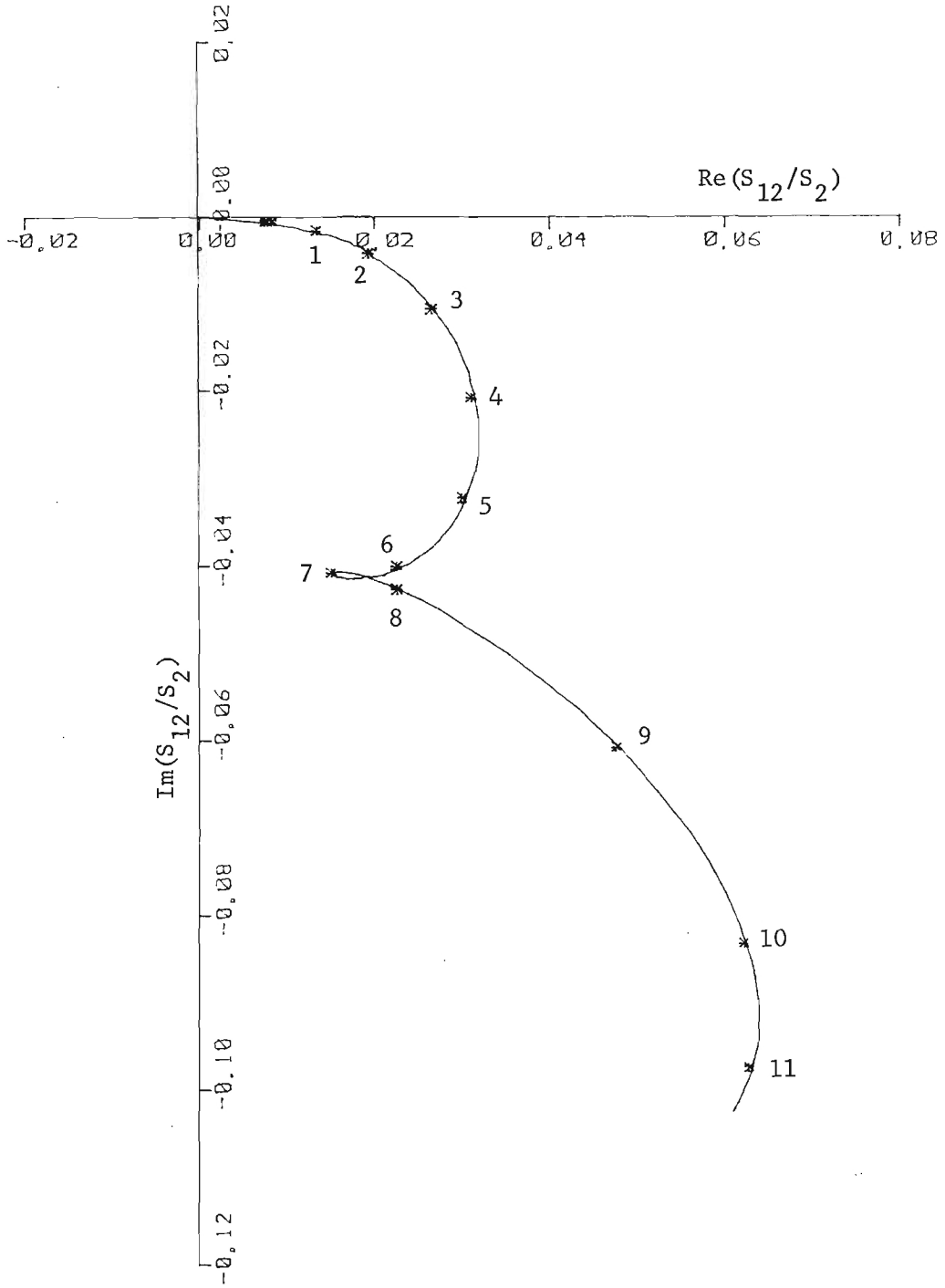

Figure 8c. Same as Figure 8a, with $\Sigma = 0.5$ m sec^{-1}.

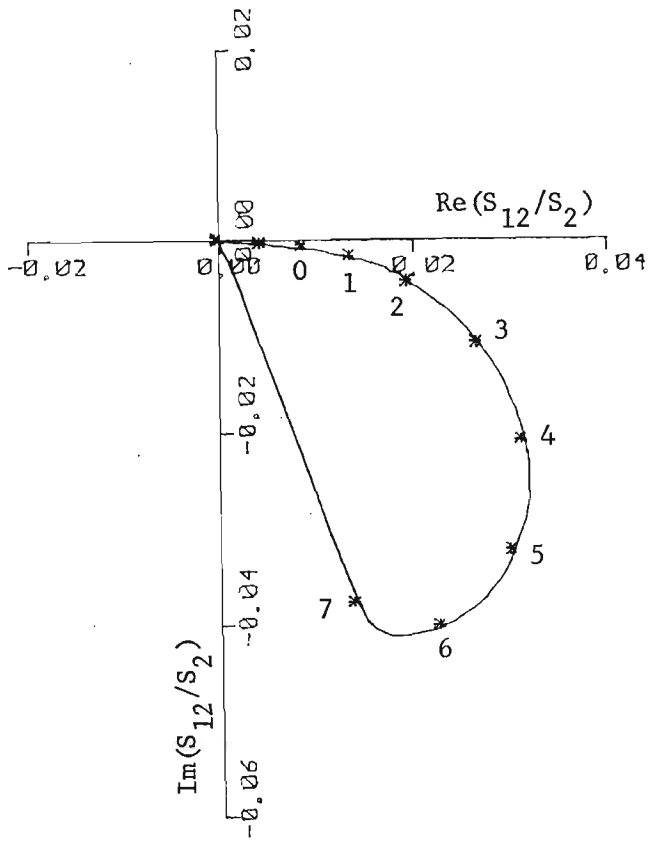

Figure 8d. Same as Figure 8c, with noise level of 50 dB below the peak of S_2. Disappearance of the relative minimum of the real part near 7 m sec^{-1} is due to the narrower Doppler velocity domain of the spectral functions at this rainfall rate, compared to those at 25 mm hr^{-1}. Compare this figure to Figure 5d.

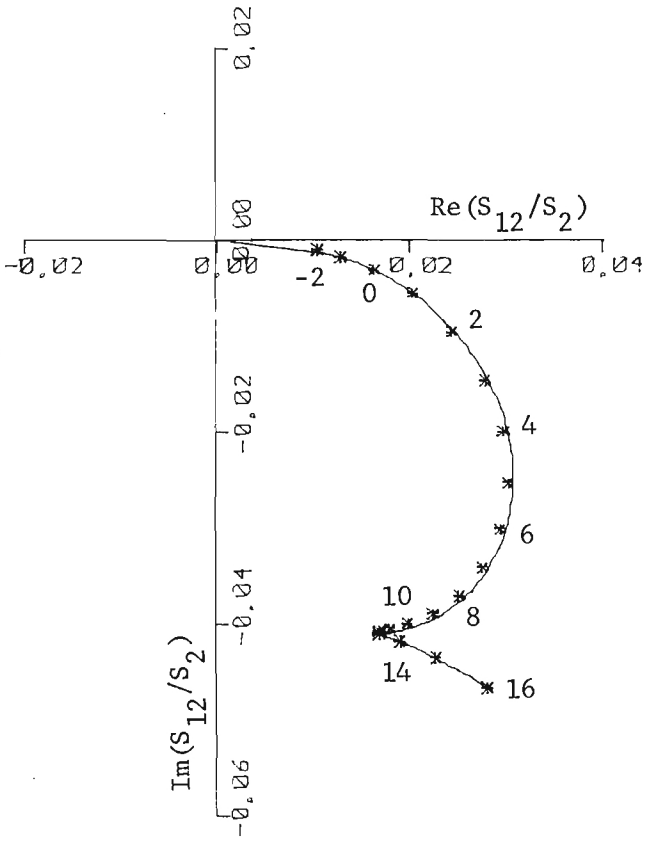

Figure 8e. Same as Figure 8a, with $\Sigma = 1.0$ m sec^{-1}.

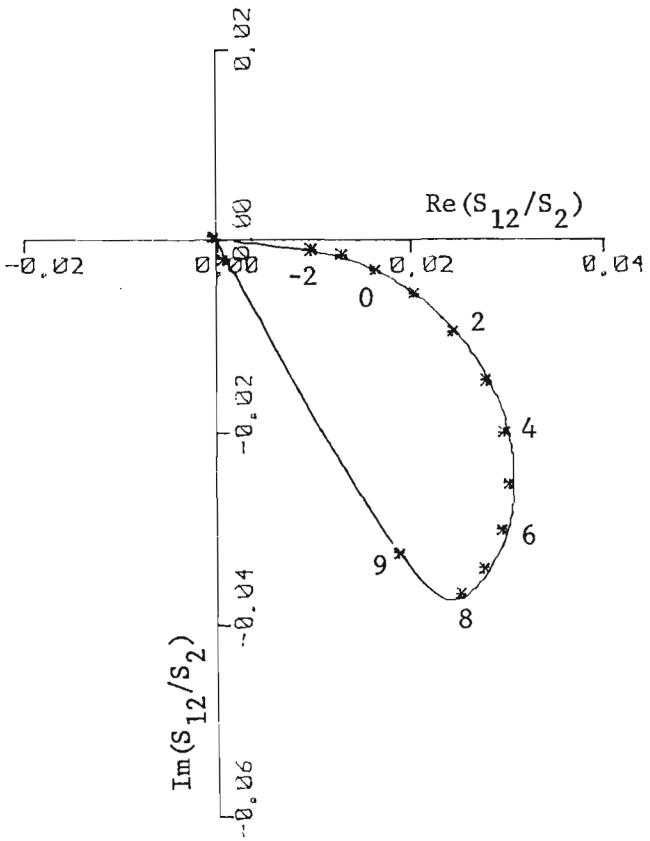

Figure 8f. Same as Figure 8e, with noise level of 50 dB below the peak of S_2.

values of Σ. With increasing air velocity variance, the full rotation of the amplitude ratio vector collapses into a small loop in the lower right quadrant (see Figure 8c) and thence into a relative minimum of the real part of S_{12}/S_2, near 6 m sec^{-1} in Figure 5c, for example, and this feature appears at progressively higher Doppler velocities. The shifting toward higher Doppler velocities is due to the increasing effect of the cross-spectral peak (near 4.7 m sec^{-1} at 25 mm hr^{-1} rainfall rate) on the cross-spectral components at higher (and lower) Doppler velocities as the velocity weighting function is broadened.

The effects of noise on the spectral power ratio and the modified cross-spectrum are shown in Figures 4, 5d, and 5f for 25 mm hr^{-1} rainfall rate and in Figures 7, 8d, and 8f for 2.5 mm hr^{-1} rainfall rate. The spectral power ratio in the presence of noise is an accurate representation of its noise-free form only in the velocity region in which the power spectrum in the transmission channel, S_1, is more than about 10 dB above the noise level. Thus, for the cases illustrated here, the spectral power ratio is of little value if the noise level were higher than about 50 dB below the peak of S_2. The modified cross-spectrum, on the other hand, is definable over almost the entire detectable bandwidth of S_2. Hence, in the presence of noise, the modified cross-spectrum would be a more useful function for analysis than the spectral power ratio. Although the relative minimum of the real part of S_{12}/S_2 is lost when $\Sigma = 1.0$ and the noise level is at -50 dB, the form of this function is preserved accurately for Doppler velocities up to about 8 m sec^{-1}.

B. Propagation Effects

The effect of propagation through rain is to increase the relative magnitude of the power spectrum S_1 in the transmission channel and to displace the cross-spectrum by a quantity corresponding to the complex propagation term $pe^{j\chi}$. The power spectra and spectral power ratio are shown in Figures 9 and 10 for 25 mm hr^{-1} rainfall rate, -50 dB noise, $\Sigma = 0.5$, and propagation distances of 0, 0.5, and 1 km. The modified cross-spectrum for the same conditions is shown in Figure 11. (The zero-distance calculation is shown in Figure 5d.) These figures illustrate the comment of Metcalf (1981) that these functions are definable over a wider velocity domain when a propagation effect is present than when it is absent. An estimate of the magnitude of the propagation term could be obtained from the power ratio near 2 m sec^{-1}, for example, on the asumption that the propagation term dominates the scattering term in this region. A more accurate estimate of the propagation term, including its magnitude and phase, could be obtained from the modified cross-spectrum by performing a best-fit matching between the propagation-shifted function and its propagation-free form. This matching would have to be performed over a limited velocity domain near the cross-spectral maximum at 4.7 m sec^{-1}, which nearly coincides with the maximum of the real part of S_{12}/S_2 in this example.

The same functions computed for 2.5 mm hr^{-1} rainfall rate are shown in Figures 12, 13, and 14. The small propagation parameters at this rainfall rate yield almost imperceptible effects on the spectral functions at distances of 1 km or less.

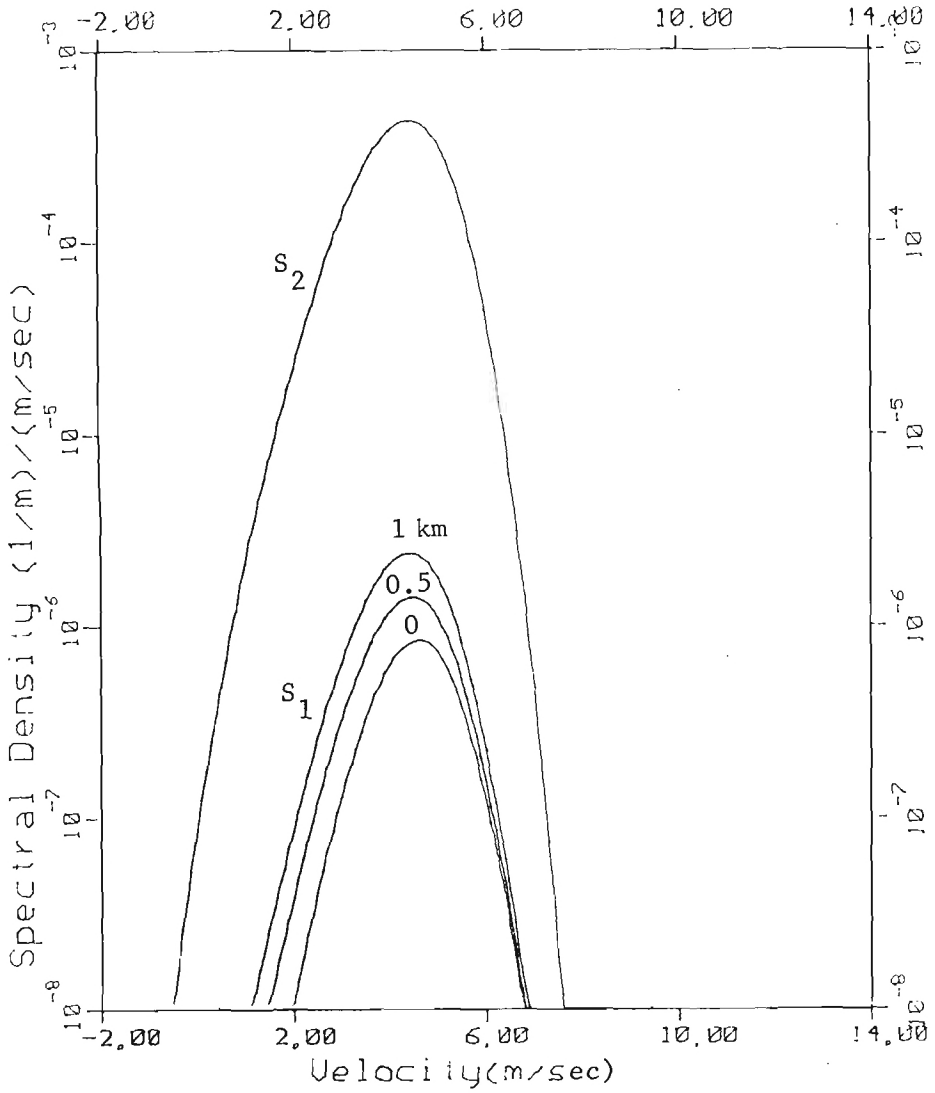

Figure 9. Power spectra in transmission and orthogonal channels at 40^{0} elevation angle in 25 mm hr^{-1} rain, with Σ = 0.5 m sec^{-1} and propagation distances of 0, 0.5, and 1 km. These spectra do not include 15 dB km^{-1} two-way power attenuation.

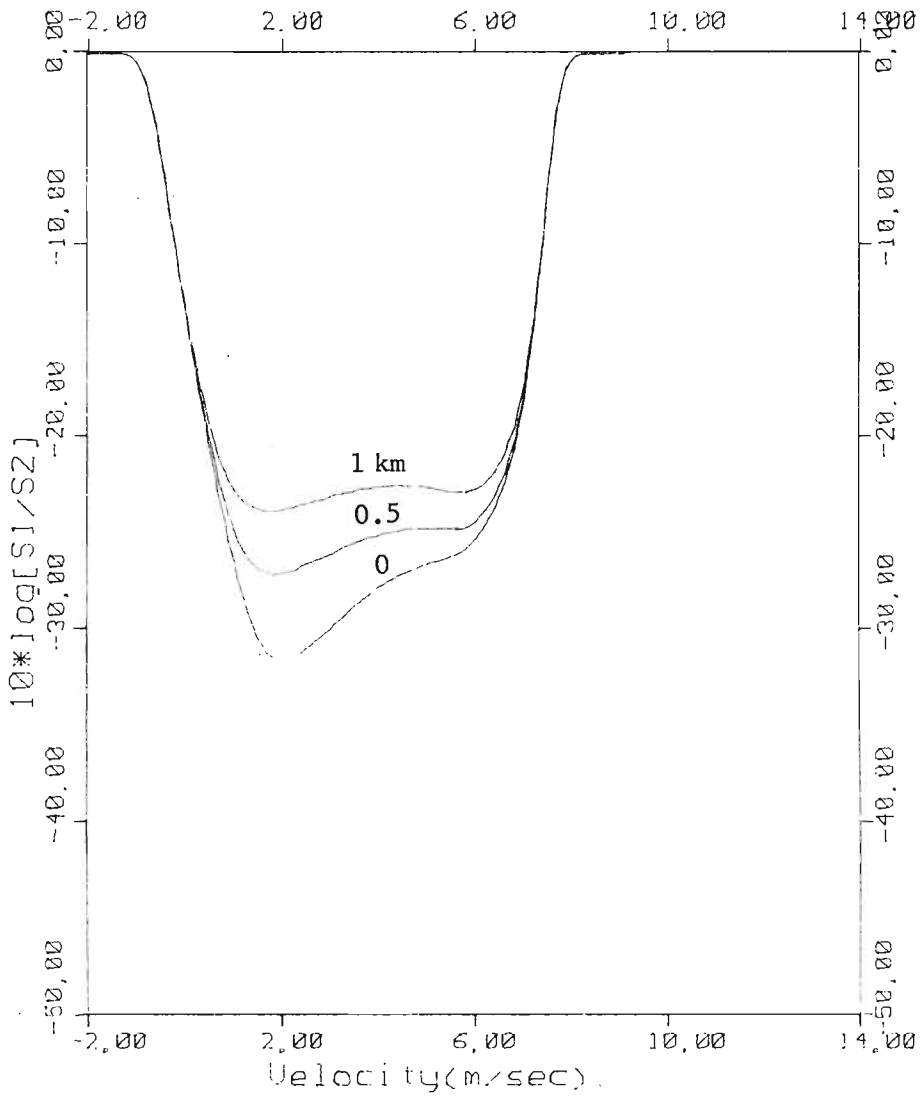

Figure 10. Spectral power ratio at 40^{o} elevation angle in 25 mm hr^{-1} rain, with Σ = 0.5 m sec^{-1}, -50 dB noise level, and propagation distances of 0, 0.5, and 1 km.

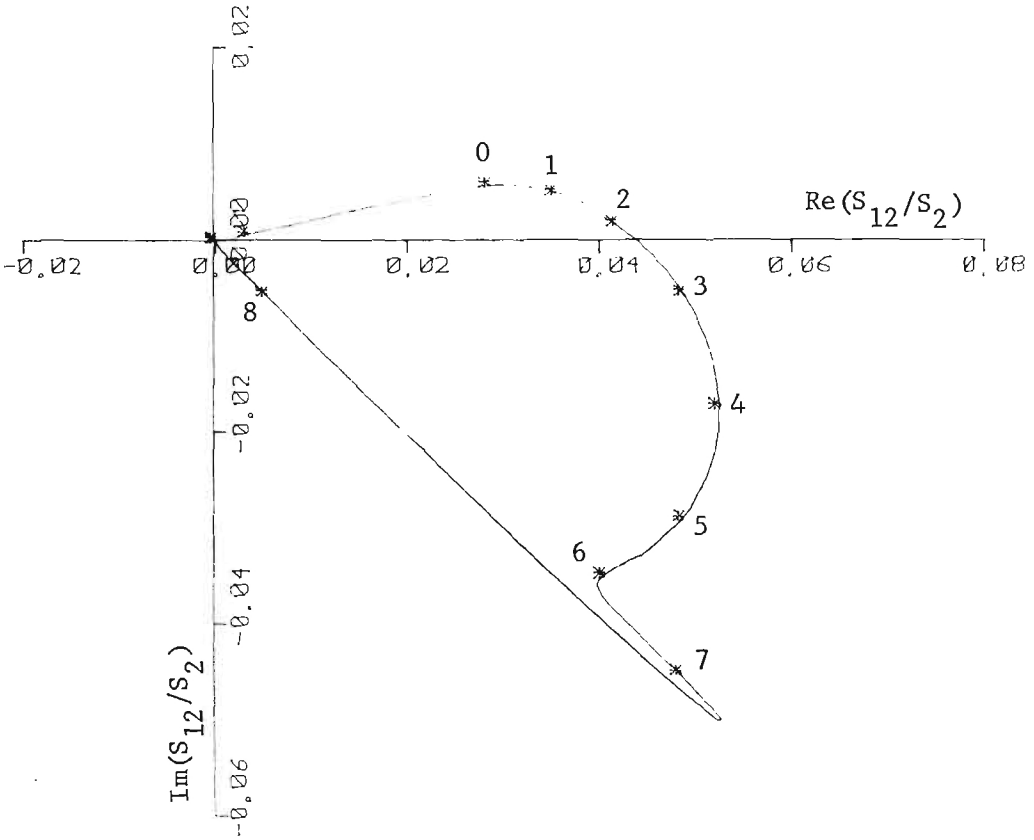

Figure 11a. Modified cross-spectrum at 40^{o} elevation angle in 25 mm hr^{-1} rain, with Σ = 0.5 m sec^{-1}, - 50 dB noise level, and 0.5 km propagation distance. Compare this figure with Figure 5d, which corresponds to the same conditions except with zero propagation distance.

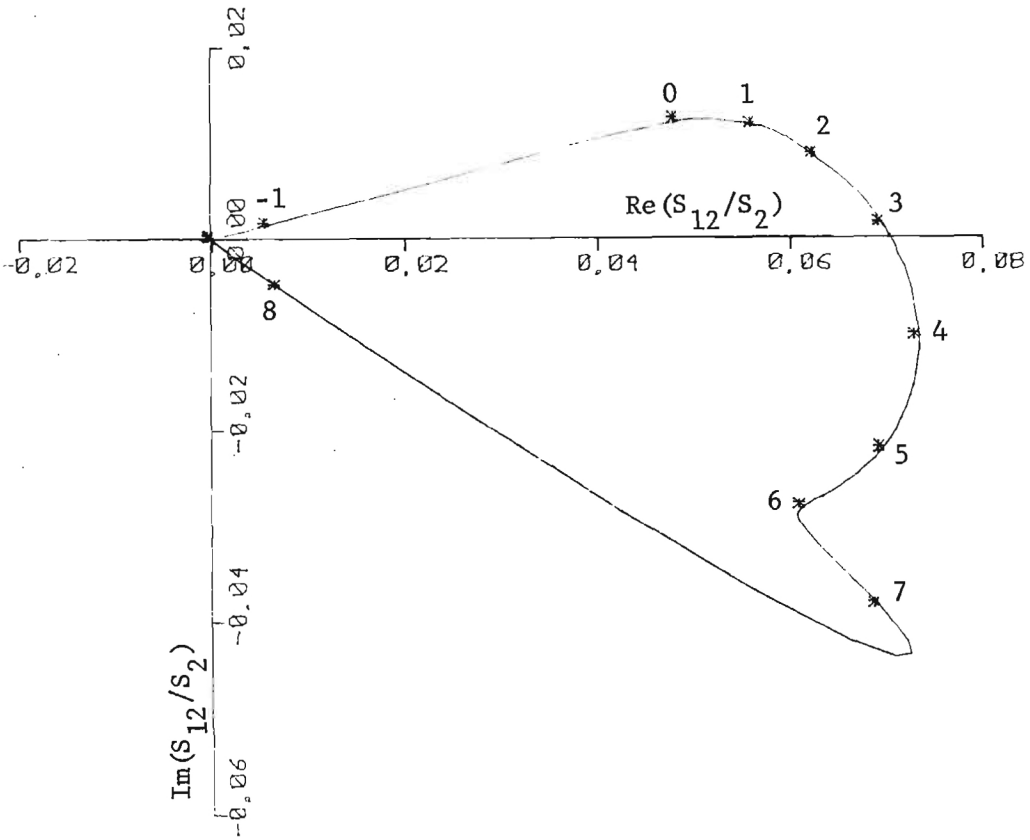

Figure 11b. Same as Figures 5d and 11a, with 1 km propagation distance. Displacement corresponds to 0.616 dB km^{-1} one-way differential attenuation and 1.35 deg km^{-1} one-way differential phase shift.

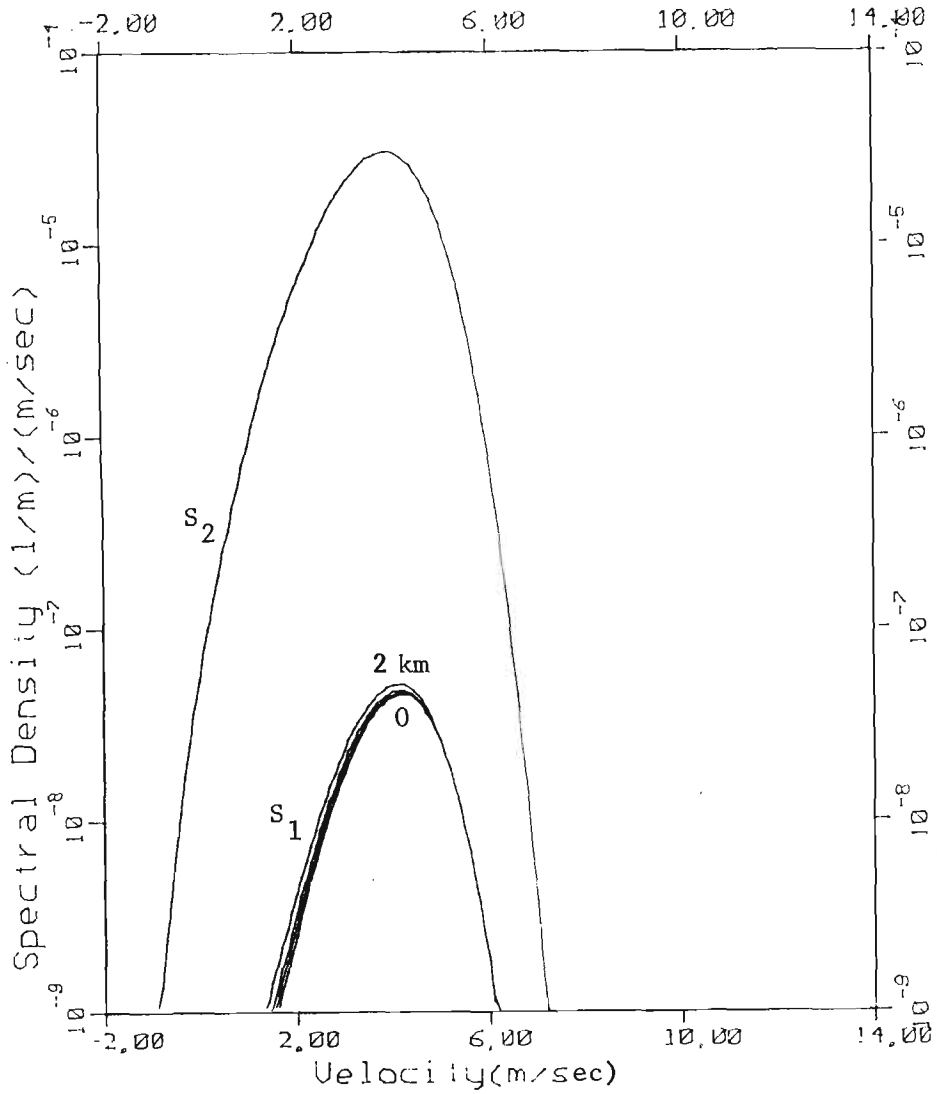

Figure 12. Power spectra in transmission and orthogonal channels at 40^0 elevation angle in 2.5 mm hr^{-1} rain, with Σ = 0.5 m sec^{-1} and propagation distances of 0, 0.5, 1, and 2 km. These spectra do not include 1.5 dB km^{-1} two-way power attenuation.

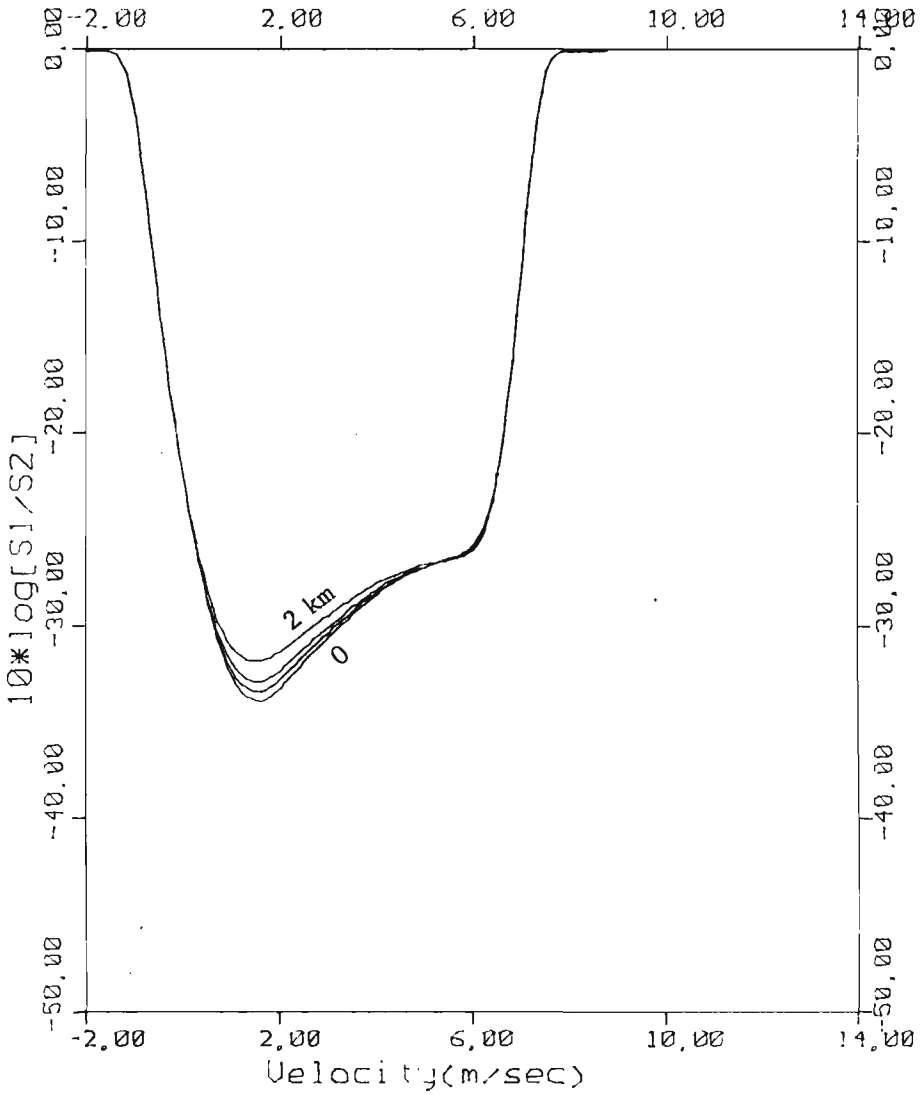

Figure 13. Spectral power ratio at 40° elevation angle in 2.5 mm hr^{-1} rain, with Σ = 0.5 m sec^{-1}, -50 dB noise level, and propagation distances of 0, 0.5, 1, and 2 km.

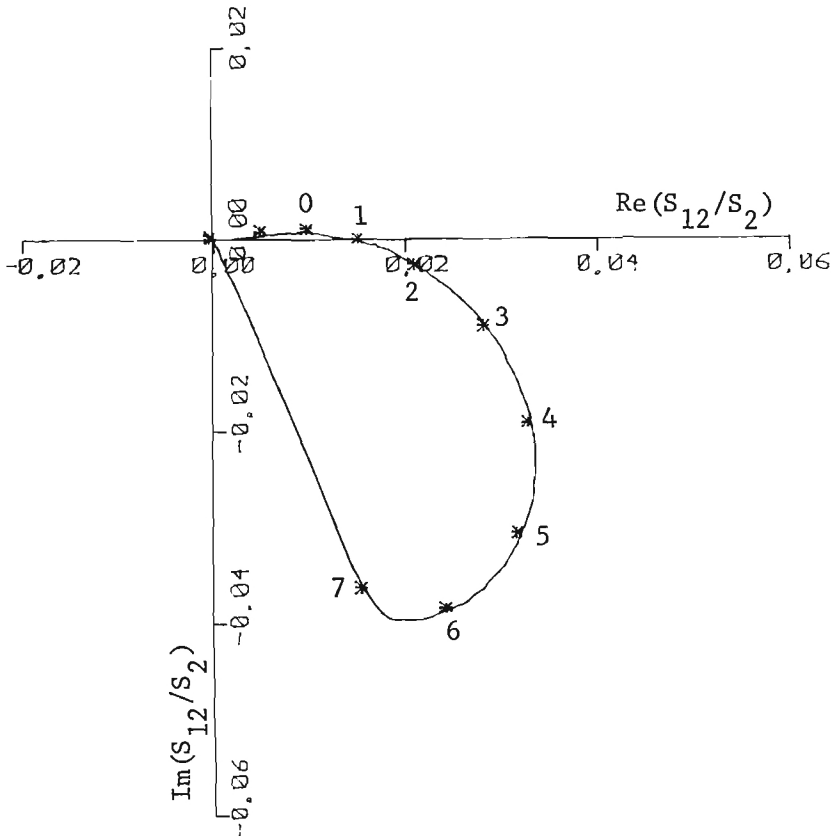

Figure 14a. Modified cross-spectrum at 40^{o} elevation angle in 2.5 mm hr^{-1} rain, with Σ = 0.5 m sec^{-1}, -50 dB noise level, and 0.5 km propagation distance. Compare this figure with Figure 8d, which corresponds to the same conditions, except with zero propagation distance.

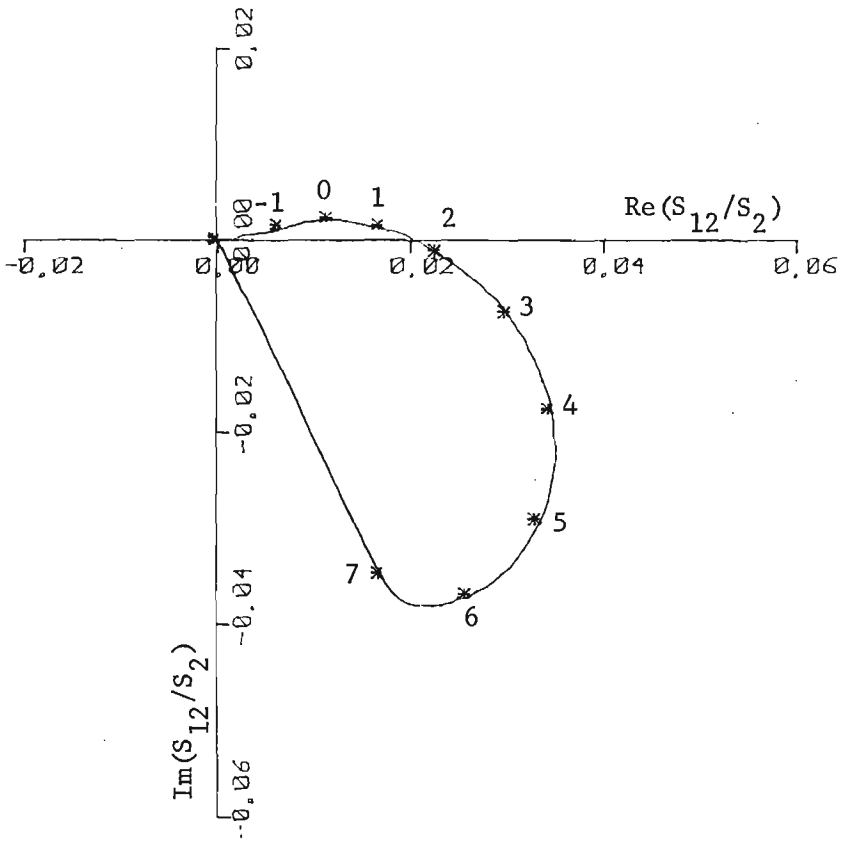

Figure 14b. Same as Figures 8d and 14a, with 1 km propagation distance.

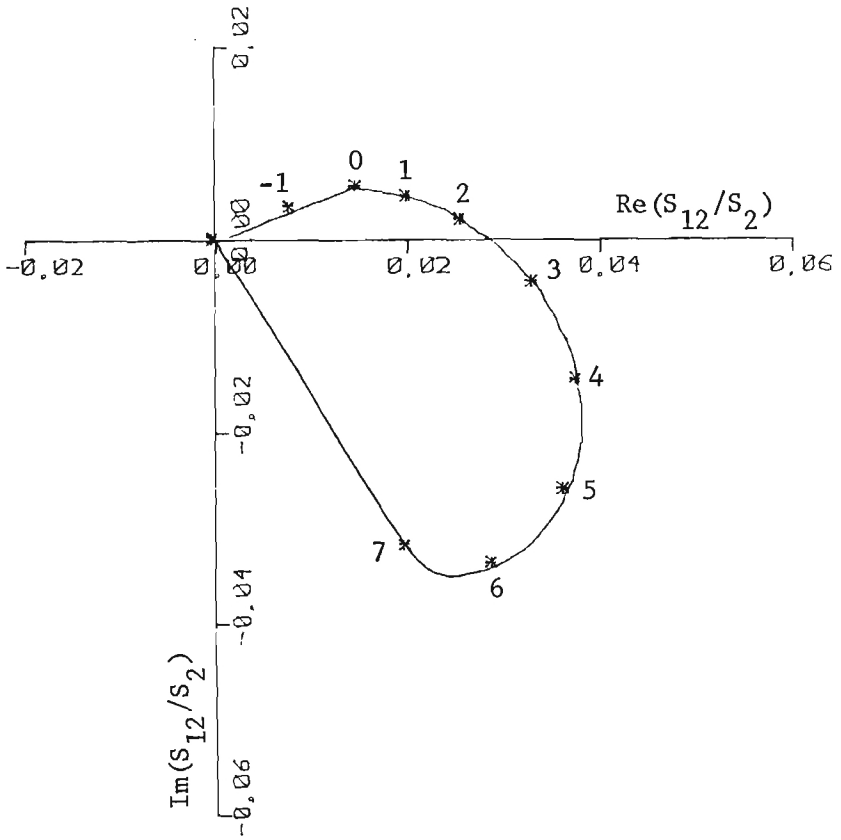

Figure 14c. Same as Figures 8d and 14a, with 2 km propagation distance. Displacement corresponds to 0.046 dB km^{-1} one-way differential attenuation and 0.306 deg km^{-1} one-way differential phase shift.

IV. SUMMARY

We have developed a model for simulating spectral functions derivable from a coherent polarization-diversity radar transmitting circular polarization and observing backscatter from rain. The spectral functions have been computed for a radar wavelength of 8.6 mm and for several values of air velocity variance and propagation distance. We performed these computations for 40^{o} elevation angle, for jointly maximizing the signal amplitude in the transmission channel (proportional to $\cos^{2}\phi$) and the Doppler velocity variance due to fall speeds (proportional to $\sin^{2}\phi$).

The results illustrate several requirements that must be met in the analysis of this type of radar data. The spectral power ratio must be more than 10 dB above the spectral noise level over an appreciable velocity domain in order that the spectral power ratio be useful for analysis. The modified cross-spectrum appears to have more analytical potential because it is not as severely affected by noise. Large values of air velocity variance, e.g., approaching 1 m^{2} sec^{-2}, limit the usefulness of the spectral functions, as certain features that might be associated with particular drop sizes are thereby shifted in Doppler velocity.

Future work with the model is planned to investigate procedures and possibilities for extracting the propagation term and for interpreting the spectral power ratio and the modified cross-spectrum in terms of raindrop size distributions, air velocity variance, and air mean velocity. While we believe that observations at 30-40^{o} elevation angle will be most desirable for the type of analysis we contemplate, calculations at other elevation angles may verify that this is so. Ultimately, we hope to use the simulations described here as aids to the interpretation of experimental radar data.

REFERENCES

Best, A. C., 1950: Empirical formulae for the terminal velocity of water drops falling through the atmosphere. Quart. J. Roy. Meteor. Soc., 76, 302-311.

Marshall, J.S., and W. M. Palmer, 1948: The distribution of raindrops with size, J. Meteor., 5, 165-166.

McCormick, G. C., and A. Hendry, 1975: Principles for the radar determination of the polarization properties of precipitation. Radio Sci., 10, 421-434.

Metcalf, J. I., 1980: Theory and experimental concepts for coherent polarization-diversity radar. Final Report, Grant ATM-7811601, National Science Foundation (Project B-529, Georgia Institute of Technology).

Metcalf, J. I., 1981: Propagation effects on a coherent polarization-diversity radar. Radio Sci., 16, in press.

Metcalf, J. I., and J. D. Echard, 1978: Coherent polarization-diversity radar techniques in meteorology. J. Atmos. Sci., 35, 2010-2019.

Oguchi, T., and Y. Hosoya, 1974: Scattering properties of oblate raindrops and cross polarization due to rain (Part II): Calculations at microwave and millimeter wave regions. J. Radio Res. Labs. (Japan), 21, 191-259.

Pruppacher, H. R., and R. L. Pitter, 1971: A semi-empirical determination of the shape of cloud and rain drops. J. Atmos. Sci., 28, 86-94.

Spilhaus, A. F., 1948: Raindrop size, shape, and falling speed. J. Meteor., 5, 108-110.

Warner, C., and R. R. Rogers, 1977: Polarization-diversity radar: Two theoretical studies. Sci. Rept. MW-90, Stormy Weather Group, McGill Univ., Montreal.